Cell Reports

Article

VEGF signaling governs the initiation of biliary-mediated liver regeneration through the PI3K-mTORC1 axis

Graphical abstract

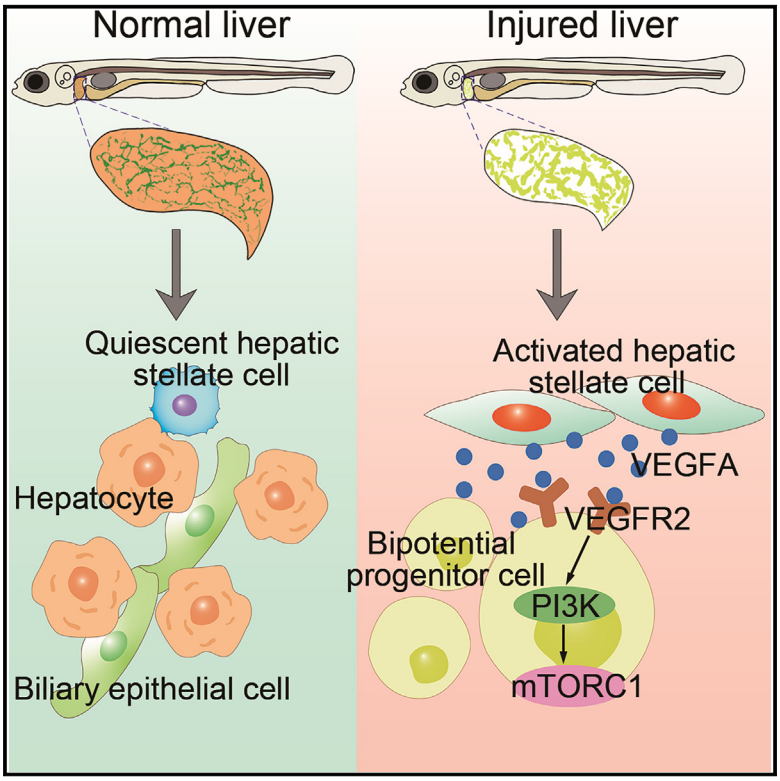

Highlights

- The expressions of *vegfaa* and *kdrl* are induced during zebrafish liver regeneration
- VEGF inhibition disrupts biliary-mediated liver regeneration in zebrafish and mice
- VEGF signaling governs biliary epithelial cell dedifferentiation via PI3K-mTORC1 axis

Authors

Pengcheng Cai, Rui Ni, Mengzhu Lv, Huijuan Liu, Jieqiong Zhao, Jianbo He, Lingfei Luo

Correspondence

lluo@swu.edu.cn

In brief

Cai et al. show that VEGF signaling is triggered to initiate biliary-mediated liver regeneration upon extreme hepatocyte injury and that the PI3K-mTORC1 axis acts as the downstream effector to control biliary epithelial cell dedifferentiation and bipotential progenitor cell proliferation.

Cai et al., 2023, Cell Reports *42*, 113028
September 26, 2023
https://doi.org/10.1016/j.celrep.2023.113028

CellPress

Cell Reports

CellPress
OPEN ACCESS

Article

VEGF signaling governs the initiation of biliary-mediated liver regeneration through the PI3K-mTORC1 axis

Pengcheng Cai,[1,3] Rui Ni,[1,3] Mengzhu Lv,[1,3] Huijuan Liu,[1] Jieqiong Zhao,[1] Jianbo He,[1] and Lingfei Luo[1,2,4,*]
[1]Institute of Developmental Biology and Regenerative Medicine, Southwest University, Beibei, Chongqing 400715, China
[2]School of Life Sciences, Fudan University, Shanghai 200438, China
[3]These authors contributed equally
[4]Lead contact
*Correspondence: lluo@swu.edu.cn
https://doi.org/10.1016/j.celrep.2023.113028

SUMMARY

Biliary epithelial cells (BECs) are a potential source to repair the damaged liver when hepatocyte proliferation is compromised. Promotion of BEC-to-hepatocyte transdifferentiation could be beneficial to the clinical therapeutics of patients with end-stage liver diseases. However, mechanisms underlying the initiation of BEC transdifferentiation remain largely unknown. Here, we show that upon extreme hepatocyte injury, *vegfaa* and *vegfr2/kdrl* are notably induced in hepatic stellate cells and BECs, respectively. Pharmacological and genetic inactivation of vascular endothelial growth factor (VEGF) signaling would disrupt BEC dedifferentiation and proliferation, thus restraining hepatocyte regeneration. Mechanically, VEGF signaling regulates the activation of the PI3K-mammalian target of rapamycin complex 1 (mTORC1) axis, which is essential for BEC-to-hepatocyte transdifferentiation. In mice, VEGF signaling exerts conserved roles in oval cell activation and BEC-to-hepatocyte differentiation. Taken together, this study shows VEGF signaling as an initiator of biliary-mediated liver regeneration through activating the PI3K-mTORC1 axis. Modulation of VEGF signaling in BECs could be a therapeutic approach for patients with end-stage liver diseases.

INTRODUCTION

The liver is an important digestive organ with high regenerative capacity. Upon partial hepatectomy or acute hepatotoxic drug exposure, hepatocyte-mediated liver regeneration, in which preexisting uninjured hepatocytes proliferate rapidly to reconstruct the liver mass, is the dominant way to repair liver function.[1] However, previous studies in zebrafish demonstrate that when hepatocytes are extremely damaged, biliary epithelial cells (BECs) first dedifferentiate into bipotential progenitor cells (BPPCs) and then redifferentiate into newly hepatocytes, and this process is named biliary-mediated liver regeneration.[2,3] The subsequent studies in mice confirmed that BEC-to-hepatocyte transdifferentiation occurs when mice suffer from chronic liver injury with compromised hepatocyte proliferation.[4,5] The process of ductular reaction, including the expansion of BECs, is the major histopathologic hallmark observed in patients with end-stage liver diseases.[6] Studies in patients with cirrhosis have identified transitional cells between BECs and hepatocytes expressing progenitor markers such as EpCAM.[7,8] Besides, the majority of distal BECs have stem-like properties in human cirrhosis,[8] implying that BECs might act as an alternative source to achieve hepatocyte regeneration in patients with end-stage liver diseases. Given orthotopic liver transplantation as the main curative approach for patients with end-stage liver diseases and the shortage of organ donors, the promotion of BEC-to-hepatocyte transdifferentiation may be beneficial to clinical therapeutics.

Zebrafish is an ideal model to study embryonic development, tissue regeneration, and several liver diseases.[9] Zebrafish embryos develop rapidly and are easy for *in vivo* imaging, making them more suitable to study biliary-derived liver regeneration compared to mice. In zebrafish, the nitroreductase-metronidazole (NTR-Mtz) system is used to achieve the extreme loss of hepatocytes, which leads to the morphological alterations of BECs to immature progenitor features. Simultaneously, the expression of BPPC markers such as *hhex*, *foxa3*, and *sox9b* are notably induced in BECs, indicating the BEC-to-BPPC dedifferentiation. Subsequently, BPPCs rapidly proliferate and redifferentiate into nascent hepatocytes and BECs.[3,10] Up to now, some essential signaling pathways that are involved in liver development, such as Wnt, Bmp, and Notch, and other critical factors such as Dnmt1, P53, Hdac1, Tel2, and FXR have been reported to regulate BPPC proliferation or redifferentiation.[2,11–15] A recent study has reported that mammalian target of rapamycin complex 1 (mTORC1) signaling is required for BEC dedifferentiation.[10] However, the regulatory mechanisms underlying the initiation of BEC dedifferentiation remain largely unknown.

Vascular endothelial growth factor (VEGF) is a kind of secreted polypeptide that binds to transmembrane tyrosine kinase VEGF receptors and subsequently induces their dimerization and

activation.[16] VEGF has been widely studied for its fundamental roles in angiogenesis, particularly with regard to its signaling through VEGFR2.[16] VEGF is mostly considered a therapeutic target for several cancers.[17] The VEGFR2 antagonists sorafenib and lenvatinib have been used for the therapy of hepatocellular carcinoma.[18,19] After partial hepatectomy, VEGF-VEGFR2 signaling promotes the angiogenic process through the regulation of endothelial cell proliferation following liver injury.[20] Those studies uncover the indispensable roles of VEGF signaling in vascular function; however, little is known about its roles beyond endothelial cells during liver regeneration.

Here, by using zebrafish and mouse liver injury models, we show that VEGF signaling controls BEC dedifferentiation and proliferation by stimulating the downstream PI3K-mTORC1 axis during biliary-mediated liver regeneration.

RESULTS

The expressions of *vegfaa* and *kdrl* are upregulated after extreme hepatocyte injury in zebrafish

Despite the essential roles of VEGF signaling in angiogenesis, whether it is involved in BEC-to-hepatocyte transdifferentiation upon extreme liver injury remains unknown. Based on the NTR-Mtz system in zebrafish, we ablated the hepatocytes using the transgenic line *Tg(lfabp:Dendra2-NTR)*, here abbreviated as *Tg(lfabp:DenNTR)*. Interrogation of our previously generated single-cell RNA sequencing (scRNA-seq) data[11] revealed that the expression of *vegfaa*, the ortholog of mammalian *Vegfa*, was notably upregulated at regeneration 0 h (R0h) after liver injury, especially in hepatic stellate cells (HSCs) (Figures 1A–1C). However, the expressions of other VEGF isoforms (*vegfab*, *vegfba*, *vegfbb*, *vegfc*, and *vegfd*) were rarely detected in the liver region (Figure S1A), indicating that *vegfaa* may be the dominant VEGF ligand that mediates VEGF signaling during liver regeneration. Then, we analyzed the expression of VEGF receptors; although all three receptors VEGFR1/Flt1, VEGFR2/Kdrl, and VEGFR3/Flt4 were highly expressed in the vascular endothelial cells (VECs), only *kdrl* showed expression in BPPCs (Figures S1B and S1C), indicating that VEGFA may directly bind to the VEGFR2 in BECs and then activate the downstream pathway. In contrast to *kdrl*, the other zebrafish *vegfr2* ortholog gene *vegfr2b/kdr* showed no obvious expression in BPPCs at R0h (Figures S1B and S1C). To quantify the expression levels of VEGF ligands and receptors in HSCs and BPPCs, we isolated hand2$^+$ HSCs and tp1$^+$ BPPCs by using the transgenic lines *Tg(hand2:GFP)*[11] and *Tg(tp1:GFP)*[21] and then performed qPCR. Similar to the scRNA-seq data, *vegfaa* showed higher expression in HSCs, while *kdrl* exhibited higher expression in BPPCs upon liver injury (Figures 1D and 1E). By performing fluorescent *in situ* hybridization (FISH), we confirmed the expressions of *vegfaa* in HSCs and *kdrl* in BPPCs (Figures 1F, 1G, and S1C). These data imply that hepatocyte-injury-induced Vegfaa may bind to VEGFR2 in BPPCs and thus participate in biliary-mediated liver regeneration.

VEGF signaling is required for BEC-to-BPPC dedifferentiation and BPPC proliferation

We next explored the roles of VEGF signaling by using the chemical AV-951, which inhibits the activity of all VEGF receptors.[22] AV-951 treatment notably reduced the regenerating liver size at R24h and R48h (Figure 2A), indicating that VEGF signaling is essential for biliary-mediated liver regeneration. During the initiation of biliary-mediated liver regeneration, BECs lose their identity and dedifferentiate into BPPCs, marked by upregulation of progenitor cell markers *foxa3*, *hhex*, and *sox9b*, as well as the morphological alteration to immature progenitor features.[10,11] Annexin A4 (Anxa4) is a well-known marker for BECs and BPPCs.[11] FISH combined with Anxa4 antibody staining showed that, compared to the control group, AV-951 treatment significantly reduced the induction of *foxa3*, *hhex*, and *sox9b* expressions in Anxa4$^+$ BECs (Figures 2B–2D). Additionally, BECs of the control group exhibited enlarged diameters at R0h, while AV-951 treatment notably counteracted this morphological alteration (Figure 2E), indicating defective BEC dedifferentiation upon VEGF inhibition.

VEGF signaling is a well-known regulator of endothelial cell proliferation,[16] so we checked if VEGF inhibition affects the proliferation of BPPCs. By performing 5-ethynyl-2′-deoxyuridine (EdU) incorporation assay combined with Anxa4 antibody staining, we found that most of the Anxa4$^+$ BPPCs were labeled by EdU signal at R8h and R24h in the control group (Figures 2F–2H), indicating the rapid proliferation of BPPCs. However, the ratio of EdU$^+$/Anxa4$^+$ cells was significantly reduced upon AV-951 treatment (Figures 2F–2H), suggesting that VEGF signaling is indispensable for BPPC proliferation.

VEGF inhibition disrupts BEC-derived hepatocyte regeneration

Given the defects in BEC dedifferentiation and BPPC proliferation upon VEGF inhibition, we hypothesized that BEC-to-hepatocyte differentiation could proceed. Whole-mount *in situ* hybridization (WISH) and qPCR results showed that at R48h, the control group exhibited high mRNA expressions of the mature hepatocyte markers *GC vitamin D binding protein* (*gc*), *ceruloplasmin* (*cp*), *hepatocyte nuclear factor 4, alpha* (*hnf4a*), and *transferrin-a* (*tfa*) in regenerating livers, while the AV-951-treated group showed few expressions of those hepatocyte markers (Figures 3A and 3B). Then, we assessed the protein expressions of Hnf4α and another hepatocyte marker, betaine-homocysteine methyltransferase (Bhmt). AV-951 treatment significantly repressed the expressions of Hnf4α and Bhmt as compared to the control group (Figures 3C and 3D), indicating defective hepatocyte regeneration upon VEGF inhibition. To further prove the effect of VEGF inhibition in biliary-mediated liver regeneration, we performed the lineage tracing assay using transgenic line *Tg(krt18:CreER;lfabp:loxP-STOP-loxP-DsRed;lfabp:DenNTR)*.[10] In the DMSO group, almost all dsRed$^+$ biliary-derived cells strongly expressed Bhmt (Figure 3E), confirming that hepatocyte regeneration is mainly contributed by BECs. However, the number and ratio of dsRed$^+$/Bhmt^{strong} hepatocytes were reduced in the AV-951 group (Figure 3E), confirming the defective BEC-to-hepatocyte transdifferentiation upon VEGF inhibition.

Selective inhibition of VEGFR2 disrupts BEC-to-hepatocyte transdifferentiation

Given the specific upregulation of *kdrl* expression in BPPCs (Figure S1C), we speculated that the involvement of VEGF signaling in biliary-mediated liver regeneration is predominately mediated

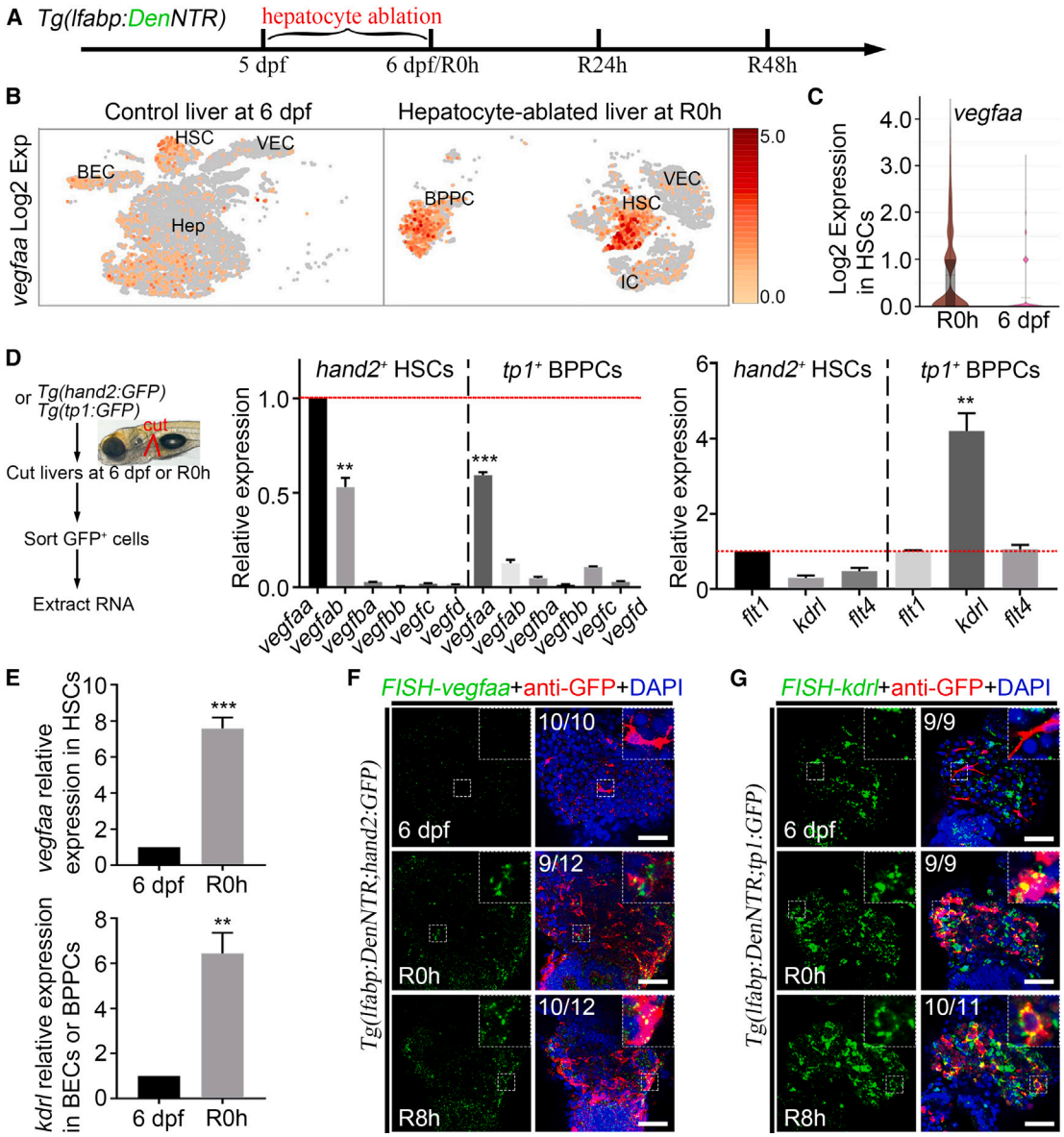

Figure 1. VEGF ligand *vegfaa* and receptor *kdrl* are induced upon extreme hepatocyte injury

(A) Experimental scheme illustrating the stages of liver regeneration.

(B) Uniform manifold approximation and projection (UMAP) showing various cell types in the livers at 6 dpf and R0h with *vegfaa* expression overlayed (red). Abbreviations: dpf, day post-fertilization; R0h, regeneration 0 h; Hep, hepatocyte; BEC, biliary epithelial cell; HSC, hepatic stellate cell; VEC, vascular endothelial cell; BPPC, bipotential progenitor cell; IC, immune cell.

(C) Quantification of *vegfaa* expression in HSCs from scRNA-seq data.

(D) Experimental scheme illustrating the process of isolating cells and extracting RNA. qPCR data showing the expression levels of VEGF ligands and receptors in HSCs and BPPCs at R0h. n = 3 technical replicates. Unpaired two-tailed Student's t test. $^{**}p < 0.01$, $^{***}p < 0.001$. Error bars represent SEM.

(E) qPCR data (top) showing the expression levels of *vegfaa* in HSCs at 6 dpf and R0h. qPCR data (bottom) showing the expression levels of *kdrl* in BECs at 6 dpf and BPPCs at R0h. n = 3 technical replicates. Unpaired two-tailed Student's t test. $^{**}p < 0.01$, $^{***}p < 0.001$. Error bars represent SEM.

(F) FISH and antibody staining showing *vegfaa* expression in GFP$^+$ HSCs at 6 dpf, R0h, and R8h under the *Tg(lfabp:DenNTR; hand2:GFP)* background. Scale bars: 50 μm.

(G) FISH and antibody staining showing *kdrl* expression in GFP$^+$ BPPCs at 6 dpf, R0h, and R8h under the *Tg(lfabp:DenNTR; tp1:GFP)* background. Scale bars: 50 μm.

See also Figure S1.

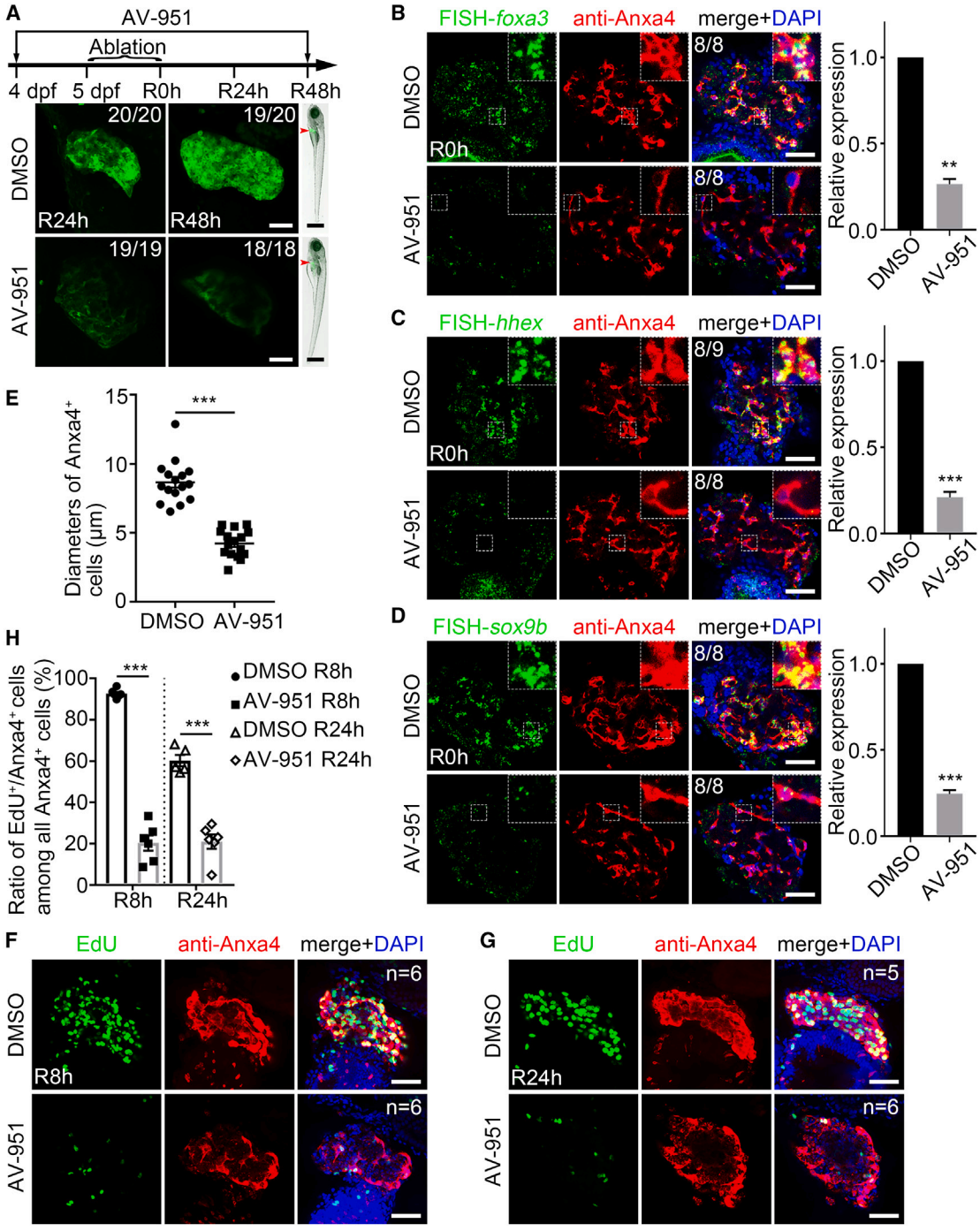

Figure 2. VEGF inhibition by AV-951 leads to defective BEC dedifferentiation and BPPC proliferation

(A) Experimental scheme showing the timeline of AV-951 treatment. Confocal projection images showing the *lfabp:DenNTR* expression at R24h and R48h. Scale bars: 50 μm. Bright-field images showing the body phenotype at R48h. Scale bars: 500 μm.

(B–D) FISH and Anxa4 antibody staining showing *foxa3* (B), *hhex* (C), and *sox9b* (D) expression in Anxa4$^+$ cells at R0h. Scale bars: 50 μm. qPCR data showing the relative expression levels of *foxa3* (B), *hhex* (C), and *sox9b* (D). n = 3 technical replicates. Unpaired two-tailed Student's t test. **p < 0.01, ***p < 0.001. Error bars represent SEM.

(E) Quantification of the diameters of Anxa4$^+$ cells at R0h. n = 16. Unpaired two-tailed Student's t test. ***p < 0.001. Error bars represent SEM.

(F and G) Confocal projection images showing EdU staining and Anxa4 antibody staining at R8h (F) and R24h (G). Scale bars: 50 μm.

(H) Quantification of the ratio of EdU$^+$/Anxa4$^+$ cells among all Anxa4$^+$ cells. n = 6 (DMSO-R8h, AV-951-R8h, and AV-951-R24h) and 5 (DMSO-R24h). Unpaired two-tailed Student's t test. ***p < 0.001. Error bars represent SEM.

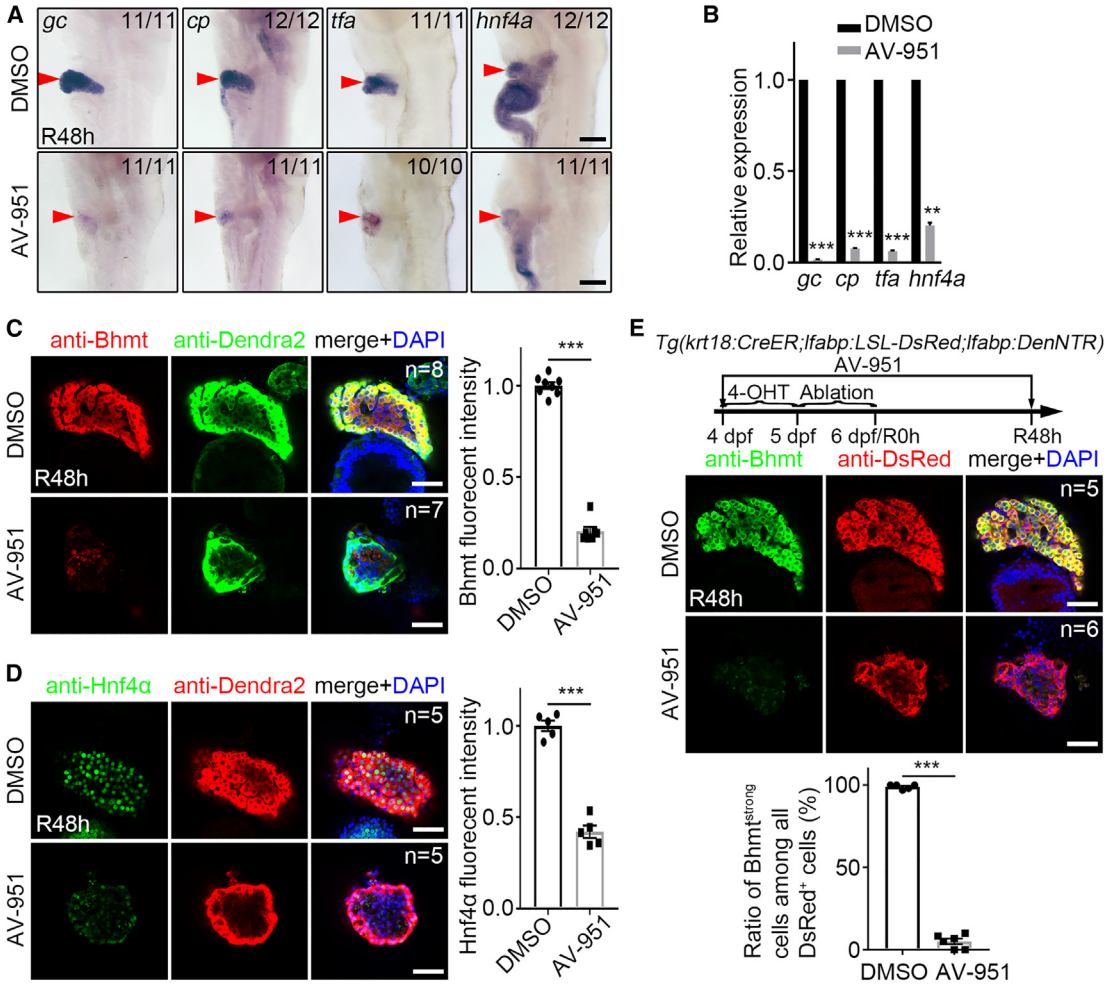

Figure 3. AV-951 treatment disrupted the differentiation of BECs to hepatocytes

(A) WISH images showing *gc*, *cp*, *tfa*, and *hnf4a* expression in regenerating livers (red arrows) at R48h. Scale bars: 100 μm.

(B) qPCR data showing the relative expression levels of *gc*, *cp*, *tfa*, and *hnf4a*. n = 3 technical replicates. Unpaired two-tailed Student's t test. **p < 0.01, ***p < 0.001. Error bars represent SEM.

(C) Single-optical section images showing Bhmt and Dendra2 expression at R48h. Scale bars: 50 μm. Quantification of the relative fluorescent intensity of Bhmt expression in liver regions. n = 8 (DMSO) and 7 (AV-951). Unpaired two-tailed Student's t test. ***p < 0.001. Error bars represent SEM.

(D) Single-optical section images showing the Hnf4α and Dendra2 expression at R48h. Scale bars: 50 μm. Quantification of the relative fluorescent intensity of Hnf4α expression in liver regions. n = 5. Unpaired two-tailed Student's t test. ***p < 0.001. Error bars represent SEM.

(E) Experimental scheme illustrating the treatments of 4-OHT and AV-951 using transgenic line *Tg(krt18:CreER; lfabp:loxP-STOP-loxP-DsRed; lfabp:DenNTR)*. Single-optical section images showing Bhmt and dsRed expression at R48h. 4-OHT, 4-hydroxytamoxifen. Scale bars: 50 μm. Quantification of the ratio of $Bhmt^{strong}$ cells among all $dsRed^{+}$ cells. n = 5 (DMSO) and 6 (AV-951). Unpaired two-tailed Student's t test. ***p < 0.001. Error bars represent SEM.

by VEGFR2. Thus, we applied another chemical, SU5416, which specifically inhibits the VEGFR2 activity.[23,24] SU5416, similar to AV-951, could indeed attenuate the phosphorylation of VEGFR2 and thus inhibit VEGF signaling in zebrafish (Figure S2A). After Mtz-induced hepatocyte injury, SU5416 treatment significantly reduced the regenerating liver size (Figure 4A), suggesting the essential roles of VEGFR2. FISH combined with Anxa4 antibody staining showed that the expressions of *foxa3*, *hhex*, and *sox9b* and the alteration of tubular morphologies were notably repressed (Figure 4B), indicating defective BEC dedifferentiation. Moreover, VEGFR2 inhibition would reduce the proliferation of BPPCs (Figure 4C), similar to the effects observed with AV-951 treatment. WISH, qPCR, and antibody stainings confirmed that the hepatocyte markers *gc*, *cp*, *tfa*, *bhmt*, and *hnf4a* were rarely expressed in SU5416-treated larvae at R48h (Figures 4D–4F), and the lineage tracing assay revealed the disrupted BEC-to-hepatocyte transdifferentiation after SU5416 treatment (Figure S2B). These data suggest that hepatocyte regeneration is blocked upon VEGFR2 inhibition. Considering the similar regenerative phenotypes upon SU5416 and AV-951 treatment and the fewer expressions of VEGFR1 and VEGFR3 in BPPCs, we conclude that VEGFR2 is the

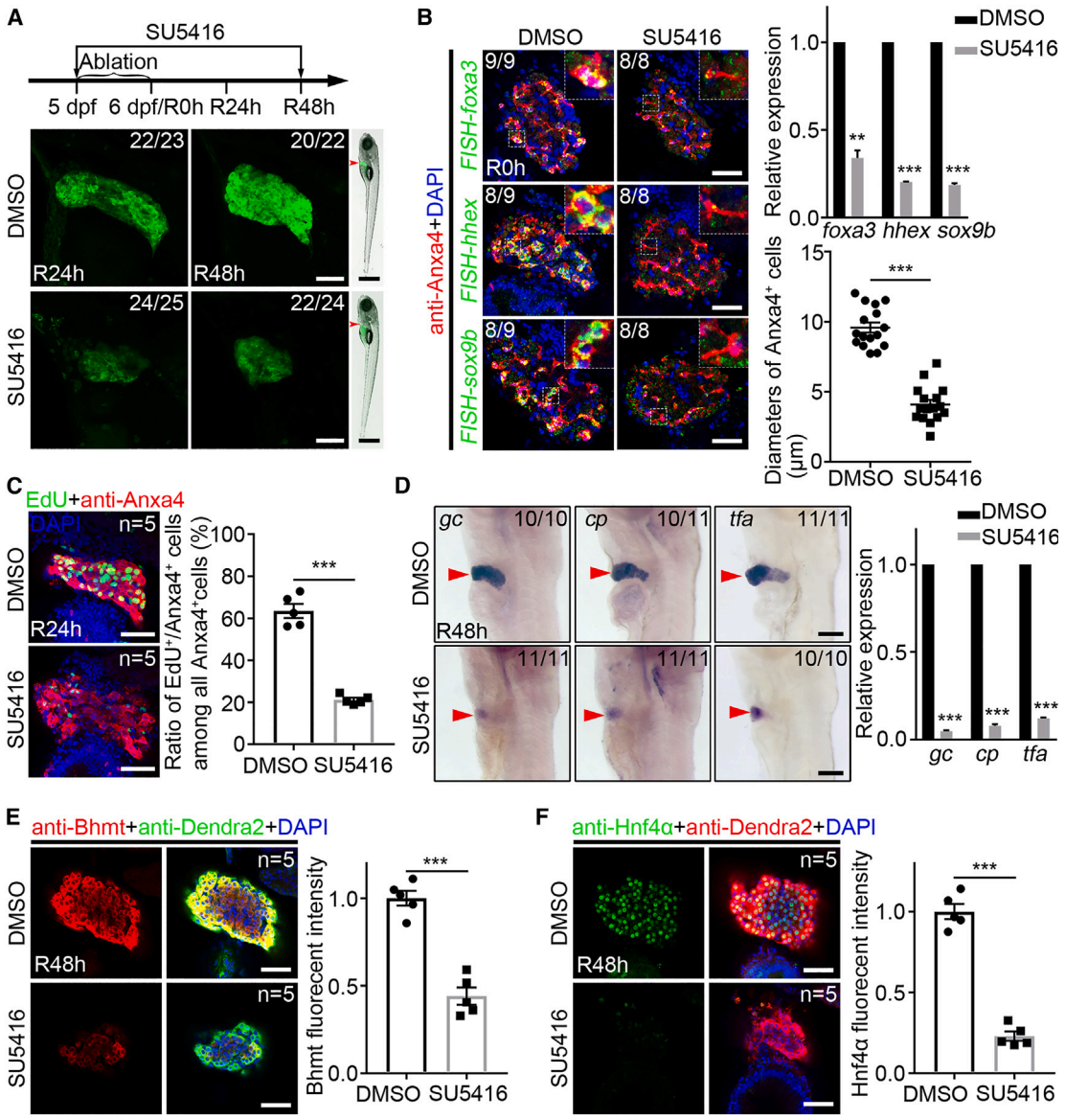

Figure 4. VEGFR2 inhibition by SU5416 causes similar regenerative defects to the AV-951 treatment

(A) Experimental scheme showing the timeline of SU5416 treatment. Confocal projection images showing the *lfabp:DenNTR* expression at R24h and R48h. Scale bars: 50 μm. Bright-field images showing the body phenotype at R48h. Scale bars: 500 μm.

(B) FISH and Anxa4 antibody staining showing *foxa3*, *hhex*, and *sox9b* expression in Anxa4$^+$ cells at R0h. Scale bars: 50 μm. qPCR data showing the relative expression levels. n = 3 technical replicates. Unpaired two-tailed Student's t test. **p < 0.01, ***p < 0.001. Error bars represent SEM. Quantification of the diameters of Anxa4$^+$ cells. n = 16. Unpaired two-tailed Student's t test. ***p < 0.001. Error bars represent SEM.

(C) Confocal projection images showing EdU staining and Anxa4 antibody staining at R24h. Scale bars: 50 μm. Quantification of the ratio of EdU$^+$/Anxa4$^+$ cells. n = 5. Unpaired two-tailed Student's t test. ***p < 0.001. Error bars represent SEM.

(D) WISH images showing *gc*, *cp*, and *tfa* expression at R48h. Scale bars: 100 μm. qPCR data showing the relative expression levels. n = 3 technical replicates. Unpaired two-tailed Student's t test. ***p < 0.001. Error bars represent SEM.

(E) Single-optical section images showing Bhmt and Dendra2 expression at R48h. Scale bars: 50 μm. Quantification of the relative fluorescent intensity of Bhmt expression in liver regions. n = 5. Unpaired two-tailed Student's t test. ***p < 0.001. Error bars represent SEM.

(F) Single-optical section images showing Hnf4α and Dendra2 expression at R48h. Scale bars: 50 μm. Quantification of the relative fluorescent intensity of Hnf4α expression in liver regions. n = 5. Unpaired two-tailed Student's t test. ***p < 0.001. Error bars represent SEM.

See also Figure S2.

main signaling receptor for VEGFA during BEC-to-hepatocyte transdifferentiation.

Genetic inactivations of *vegfaa* and *kdrl* cause similar liver regenerative defects as VEGF antagonist treatments

The expression of *vegfaa* was notably induced in HSCs after extreme hepatocyte injury (Figure 1), implying that Vegfaa is the predominant ligand for VEGFR activation. The zebrafish *vegfaa* mutant shows severe vascular defects in the early stages.[25] Therefore, to disrupt *vegfaa*-stimulated VEGF signaling, we engineered a heat-shock-induced transgenic line expressing a dominant-negative *vegfaa* isoform (*dnvegfaa*), which could effectively block VEGFA signaling.[26–28] Upon liver injury, induction of *dnvegfaa* expression led to defective liver regeneration at R24h and R48h (Figure 5A). BEC dedifferentiation was also impaired upon *dnvegfaa* overexpression, as reflected by the lower expressions of *foxa3*, *hhex*, and *sox9b* (Figure 5B). Likewise, proliferation of BPPCs was notably reduced in the *dnvegfaa*-overexpressed group (Figure 5C). WISH and antibody staining results confirmed that the hepatic markers *gc*, *cp*, and *bhmt* were notably reduced (Figures 5D and 5E), indicating the disruption of hepatocyte regeneration upon VEGFA inactivation. The general *dnvegfaa* overexpression could induce more redundant inhibitory VEGF proteins and might affect other cell types, so we constructed the transgenic line *Tg(krt18:Tet3G;Tre3G:dnvegfaa-P2A-DsRed)* to specifically overexpress *dnvegfaa* in BECs based on the Tet-On system.[15] BEC-specific *dnvegfaa* overexpression caused similar liver-regenerative phenotypes to general *dnvegfaa* overexpression (Figure S3A), confirming that the activation of VEGF signaling in BECs is essential for BEC-to-hepatocyte transdifferentiation.

Despite the roles of VEGFR2 having been adequately proved by the antagonist treatments, we generated the *kdrl* mutant to confirm it in a genetic way (Figures S3B and S3C). Unlike the *Kdr* mutant mice that die *in utero* due to severe vascular developmental defects, zebrafish *kdrl* mutants could survive to 7 days post-fertilization (dpf) and exhibited milder vascular defects.[29] Consistent with the previous study,[30] liver development was relatively normal in the *kdrl* mutant (Figure 6A). To detect the regenerative phenotype at later stages, we ablated the hepatocytes of *kdrl* mutants from 4 dpf. Similar to the effects of chemical treatments, *kdrl* mutants exhibited smaller regenerating livers (Figure 6A). Further experiments showed a notable reduction in the expressions of *foxa3*, *hhex*, and *sox9b* at R0h (Figure 6B), disruption of BPPC proliferation at R24h (Figure 6C), and significant inhibition of hepatocyte regeneration at R48h in the *kdrl* mutant (Figures 6D and 6E). To exclude the unspecific effects of the *kdrl* mutation, we also generated a Tet-On-based transgenic line, *Tg(krt18:Tet3G;Tre3G:dnkdrl-P2A-DsRed)*, that expresses a dominant-negative *kdrl* isoform (*dnkdrl*) specifically in BECs. This isoform is capable of orientating to the membrane but lacks intracellular protein kinase activity (Figure S3C). Similar to the *kdrl* mutant, BEC-specific *dnkdrl* overexpression could effectively inhibit BEC dedifferentiation, BPPC proliferation, and hepatocyte regeneration (Figures S3D–S3G), indicating that VEGFR2 serves as the primary transducer of VEGF signaling that governs biliary-mediated liver regeneration.

VEGF signaling governs biliary-mediated liver regeneration through PI3K-mTORC1 axis

Upon VEGF binding and receptor dimerization, VEGFR2 undergoes autophosphorylation, thus activating downstream signaling pathways such as PI3K-mTOR.[16] Phosphorylated ribosomal S6 protein (p-RS6) is a well-known downstream effector of mTORC1,[31] and its expression level reflects the activation of mTORC1 signaling.[10] Consistent with the previous study,[10] we validated that mTORC1 signaling is highly activated at R0h and R8h (Figure S4A) and that mTORC1 inhibition by rapamycin treatment would disrupt BEC-to-hepatocyte transdifferentiation (Figures S4B and S4C). Thus, we hypothesized that VEGF regulates biliary-mediated liver regeneration by activating the PI3K-mTORC1 axis. To confirm if PI3K signaling acts upstream of mTORC1 and is required for liver regeneration, we first analyzed the expression of p-RS6 after the treatment of PI3K inhibitor LY294002. PI3K inhibition could indeed completely block the expression of p-RS6 (Figure S4D), indicating that the phosphorylation of RS6 is a good indicator of PI3K-mTORC1 axis activation. Moreover, LY294002 treatment caused similar regenerative defects to VEGF or mTORC1 inhibition, including disrupted BEC dedifferentiation, compromised BPPC proliferation, and reduced hepatocyte regeneration (Figures S5A–S5F). These data indicate that the PI3K-mTORC1 axis regulates BEC dedifferentiation and that it is essential for liver regeneration.

To prove the hypothesis that the PI3K-mTORC1 axis is regulated through VEGF signaling, we performed p-RS6 antibody staining and found that p-RS6 was highly expressed in BPPCs of the control group, while it was notably decreased upon VEGF pharmacological inhibition, *dnvegfaa* overexpression, and *kdrl* mutation (Figures 7A, S4E, and S4F), suggesting the requirement of VEGF signaling in PI3K-mTORC1 axis activation. To validate the regulatory axis, we applied a potential PI3K agonist 1,3-dicaffeoylquinic acid (DQA).[32] The DQA treatment could partially rescue the reduced expression of p-RS6 upon VEGF inhibition (Figure 7A), confirming that the PI3K-mTORC1 axis acts downstream of VEGF signaling. Moreover, PI3K activation notably improved the expressions of BPPC markers at R0h and of the hepatic markers at R48h (Figures 7B, 7C, and 7E) and partially rescued defective BPPC proliferation at R24h (Figure 7D). To further confirm the regulatory axis, we applied another PI3K agonist, 740 Y-P,[33] which could also ameliorate the deficient regenerative phenotype caused by VEGF inhibition (Figures S6A–S6D). Taken together, these data suggest that VEGF signaling controls the initiation of biliary-mediated liver regeneration through the PI3K-mTORC1 axis (Figure 7F).

VEGF signaling regulates oval cell activation and BEC-to-hepatocyte differentiation in mice

The critical roles of VEGF signaling in BEC dedifferentiation and BPPC proliferation in zebrafish prompted us to investigate its roles in oval cell activation in mammals. The choline-deficient, ethionine-supplemented (CDE)-diet-induced mouse liver injury model, in which oval cells are mostly derived from BECs,[34,35] was used for this investigation. 2-month old mice were fed a CDE diet for 14 days, and AV-951 or PBS control was intraperitoneally injected daily from days 8 to 13 (Figure S7A). To examine the oval activation upon VEGF inhibition, we performed antibody

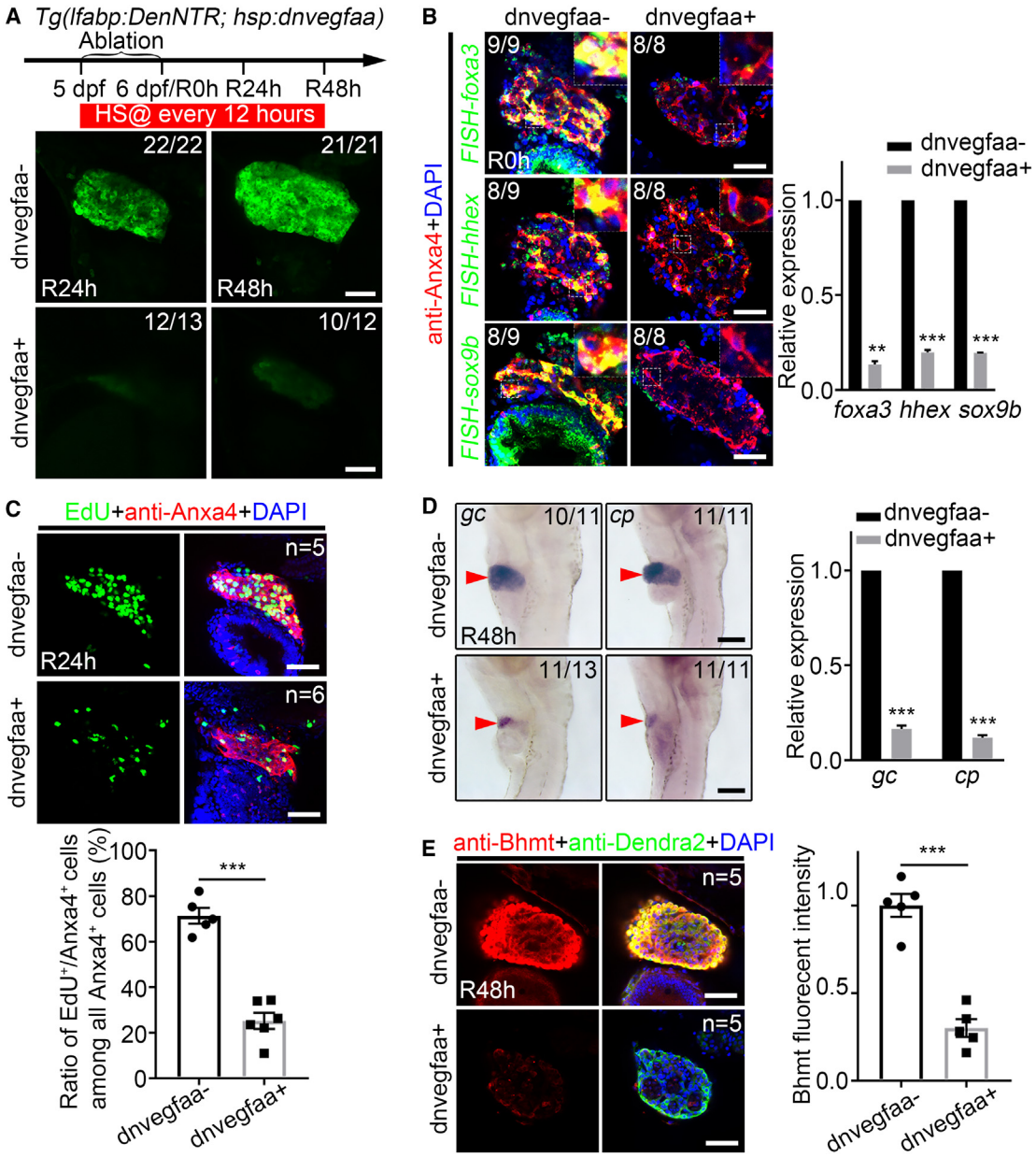

Figure 5. Genetic inactivation of *vegfaa* inhibits biliary-mediated liver regeneration

(A) Experimental scheme showing the timeline of hepatocyte ablation and heat shock. Confocal projection images showing *lfabp:DenNTR* expression. Scale bars: 50 μm.

(B) FISH and Anxa4 antibody staining showing *foxa3*, *hhex*, and *sox9b* expression in Anxa4$^+$ cells at R0h. Scale bars: 50 μm. qPCR data showing the relative expression levels. n = 3 technical replicates. Unpaired two-tailed Student's t test. **p < 0.01, ***p < 0.001. Error bars represent SEM.

(C) Confocal projection images showing EdU staining and Anxa4 antibody staining at R24h. Scale bars: 50 μm. Quantification of the ratio of EdU$^+$/Anxa4$^+$ cells. n = 5 (dnvegfaa−) and 6 (dnvegfaa+). Unpaired two-tailed Student's t test. ***p < 0.001. Error bars represent SEM.

(D) WISH images showing *gc* and *cp* expression at R48h. Scale bars: 100 μm. qPCR data showing the relative expression levels. n = 3 technical replicates. Unpaired two-tailed Student's t test. ***p < 0.001. Error bars represent SEM.

(E) Single-optical section images showing Bhmt and Dendra2 expression at R48h. Scale bars: 50 μm. Quantification of the relative fluorescent intensity of Bhmt expression in liver regions. n = 5. Unpaired two-tailed Student's t test. ***p < 0.001. Error bars represent SEM.

See also Figure S3.

stainings for oval cell marker Sox9 and BEC marker CK19. In the control group, a large number of Sox9$^+$ and CK19$^+$ cells expanded into the hepatic lobule (Figures S7B and S7C), indicating the activation of oval cells. However, these oval cells were significantly decreased in the AV-951-treated group as compared to the control (Figures S7B and S7C), suggesting

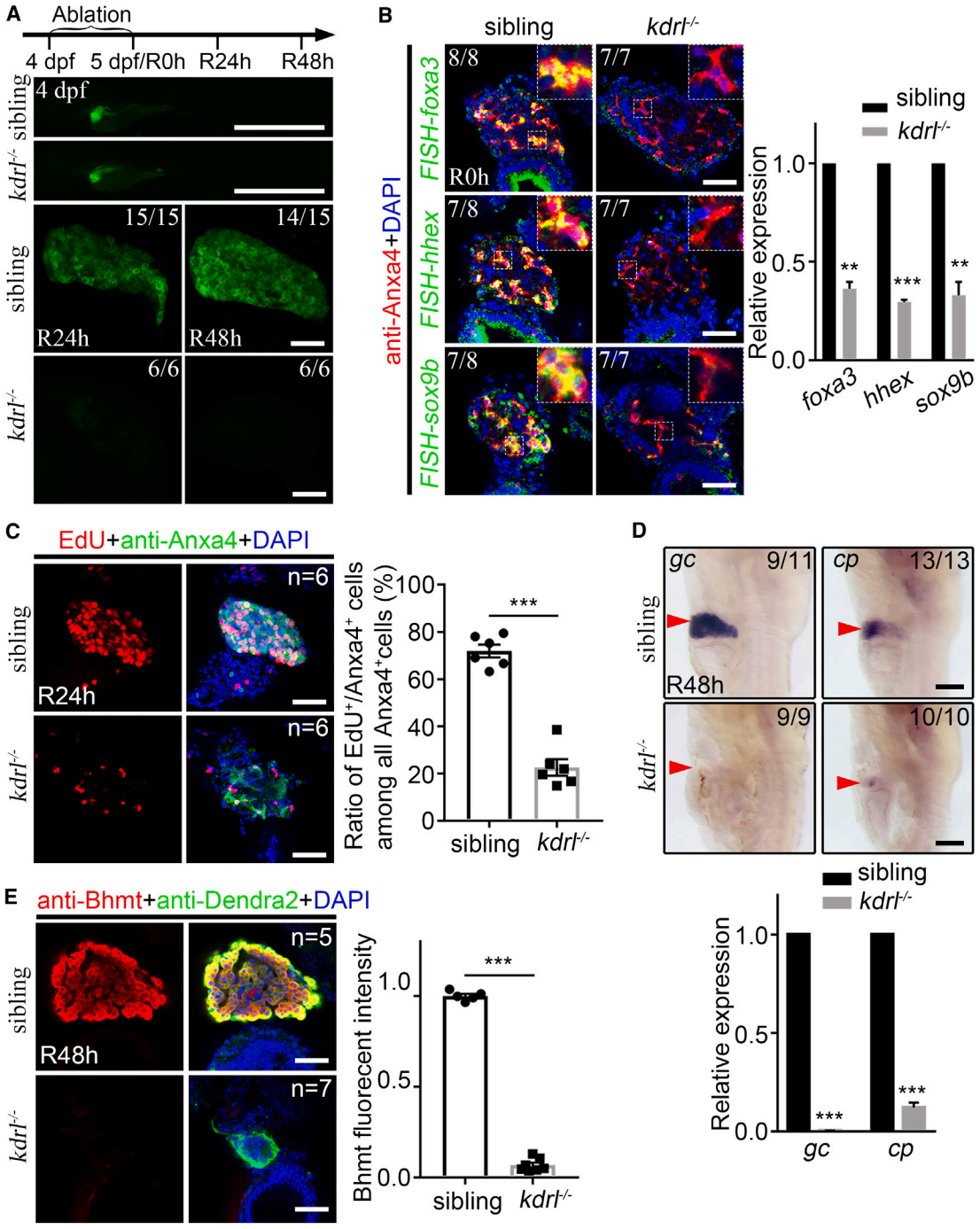

Figure 6. Knockout of *kdrl* disrupts BEC-to-hepatocyte transdifferentiation

(A) Experimental scheme illustrating the stages of hepatocyte ablation. Fluorescent images showing the developmental livers at 4 dpf. Confocal projection images showing *lfabp:DenNTR* expression at R24h and R48h. Scale bars: 1 mm (4 dpf) and 50 μm (R24h and R48h).

(B) FISH and Anxa4 antibody staining showing *foxa3*, *hhex*, and *sox9b* expression in Anxa4$^+$ cells at R0h. Scale bars: 50 μm. qPCR data showing the relative expression levels. n = 3 technical replicates. Unpaired two-tailed Student's t test. **p < 0.01, ***p < 0.001. Error bars represent SEM.

(C) Confocal projection images showing EdU staining and Anxa4 antibody staining at R24h. Scale bars: 50 μm. Quantification of the ratio of EdU$^+$/Anxa4$^+$ cells. n = 6. Unpaired two-tailed Student's t test. ***p < 0.001. Error bars represent SEM.

(legend continued on next page)

that VEGF inhibition disrupts oval cell activation. Moreover, in the control group, most of the cells with small nuclei surrounding the portal area, a feature of BECs/oval cells, exhibited Ki67$^+$ (Figure S7D). However, these Ki67$^+$ cells were greatly reduced in the AV-951-treated group (Figure S7D). These data indicate that VEGF signaling regulates the activation and proliferation of BEC-derived oval cells upon mouse liver injury, as in the zebrafish.

To investigate the roles of VEGF signaling in mouse BEC-derived hepatocyte regeneration, we applied a well-constructed mouse model based on hepatocyte-specific P21 overexpression.[4] By using *OPN*^{CreER}*tdTomato*^{LSL} lineage-tracing mice combined with tamoxifen injection, the BEC-derived hepatocytes would be labeled by tdTomato. After 15 days of recovery upon methionine/choline-deficient (MCD)-diet-induced liver injury, we observed that BEC-derived tdTomato$^+$ hepatocyte-shaped cells, which also express Hnf4α, were reduced in the AV-951 and rapamycin-treated groups (Figures S7E and S7F), suggesting the disrupted BEC-to-hepatocyte differentiation upon VEGF and mTORC1 inhibitions. To further confirm our findings, we used another mouse model in which hepatic-specific β-catenin/Ctnnb1 deletion provokes the differentiation of hepatocytes from BECs upon severe liver injury.[36] By using *Ctnnb1*$^{flox/flox}$*tdTomato*^{LSL} mice, AAV8-TBG-Cre injection could induce the conditional knockout of *Ctnnb1* in hepatocytes and the expression of tdTomato in pre-existing hepatocytes. After CDE-induced liver injury, the newly BEC-derived hepatocytes are marked as Ctnnb1$^+$ and tdTomato$^-$.[36] Similar to the P21-overexpression model, VEGF inhibition significantly reduced the generation of BEC-derived Ctnnb1$^+$/tdTomato$^-$ hepatocytes (Figure S7G), confirming that VEGF signaling is required for biliary-mediated liver regeneration in mice.

DISCUSSION

Given the compromised hepatocyte proliferation upon extreme liver injuries, the process of biliary-mediated liver regeneration is of great scientific and clinical interest for patients with chronic liver diseases, particularly patients with end-stage liver diseases. In this study, we discover the essential roles of VEGF signaling in initiating biliary-mediated liver regeneration. Our data show that *vegfaa* expression in HSCs and *kdrl* expression in BECs would be induced upon zebrafish extreme hepatocyte injury. Pharmacological inhibition and genetic inactivation of VEGF signaling impaired both BEC dedifferentiation and BPPC proliferation. Moreover, VEGF inhibition disrupted oval cell activation in the CDE-induced mouse liver injury model, implying that the finding in zebrafish is conserved in mammals.

In hepatocyte-mediated liver regeneration, VEGF signaling regulates the proliferation of endothelial cells, which secrete pro-regenerative factors that are essential for liver regeneration.[20] Surprisingly, VEGF inhibition would not affect the number and morphogenesis of endothelial cells after extreme hepatocyte injury (Figure S2C), indicating that VEGF signaling may directly regulate BEC transdifferentiation, which differs from its roles in hepatocyte-mediated liver regeneration. This difference could be explained by the different damage levels of endothelial cells. Endothelial cells proliferate robustly to rebuild the damaged vascular network in hepatocyte-derived liver regeneration, while in the extreme hepatocyte injury model, endothelial cells are hardly damaged (Figure S2C). However, whether some pro-regenerative factors are secreted by endothelial cells and promote BEC transdifferentiation needs to be further investigated.

Despite VEGF signaling being reported to regulate BEC proliferation in the rat bile duct ligation (BDL) model,[37,38] our work discovers new roles of VEGF signaling that differ from the previous study. In the BDL model, BECs proliferate rapidly to compensate for the structural and functional derangement of the intrahepatic biliary tree without changing the cell fate, and VEGF signaling just regulates the proliferation of BECs. However, in biliary-mediated liver regeneration, BECs first dedifferentiate into the progenitor cell and then proliferate. Thus, the regulation of VEGF signaling is on progenitor cell proliferation, which is validated by the requirements of VEGF in mouse oval cell proliferation (Figure S7). However, our and previous[10] studies both show that defective BEC dedifferentiation is accompanied by compromised BPPC proliferation, indicating the main regulation of BEC dedifferentiation by VEGF signaling. Indeed, progenitor cells own much higher regenerative capacity,[6] and the defects in the transition of BECs to BPPCs could logically cause compromised proliferation.

HSCs, which are closely associated with liver fibrosis, have been shown to highly express VEGF ligands during activation.[39,40] Although earlier studies in mice have revealed the fibrogenic effects of VEGF through multiple mechanisms,[40,41] VEGF is also reported to be essential for liver repair and fibrosis resolution,[42] implying that the activated HSCs may play positive roles through secreting VEGF during liver regeneration. Upon liver injury in zebrafish, the number of HSCs increased notably, and the morphology of HSCs changed to be more elongated (Figure 1F), a feature of activated HSCs.[43] Similarly, the expression of *vegfaa* was induced in HSCs upon extreme hepatocyte injury, suggesting that activated HSCs are potential sources for VEGF ligands in both mammals and zebrafish. Despite the fact that *vegfaa* is the dominant VEGF ligand that is upregulated upon liver injury, the other three ligands *vegfab*, *vegfba*, and *vegfc* showed expressions to a certain degree in HSCs and BPPCs (Figure S1A). Thus, it is not possible to exclude the involvement of other VEGF ligands in the activation of VEGF signaling, as maybe these ligands could also bind to their receptors and activate the downstream signaling pathways.

Consistent with the findings in endothelial cells,[16] VEGFR2 acts as the main transducer of VEGF signaling during BEC-to-hepatocyte transdifferentiation. We only detected the upregulation of

(D) WISH images showing *gc* and *cp* expression at R48h. Scale bars: 100 μm. qPCR data showing the relative expression levels. n = 3 technical replicates. Unpaired two-tailed Student's t test. ***p < 0.001. Error bars represent SEM.
(E) Single-optical section images showing Bhmt and Dendra2 expression at R48h. Scale bars: 50 μm. Quantification of the relative fluorescent intensity of Bhmt expression in liver regions. n = 5 (sibling) and 7 (*kdrl*$^{-/-}$). Unpaired two-tailed Student's t test. ***p < 0.001. Error bars represent SEM.
See also Figure S3.

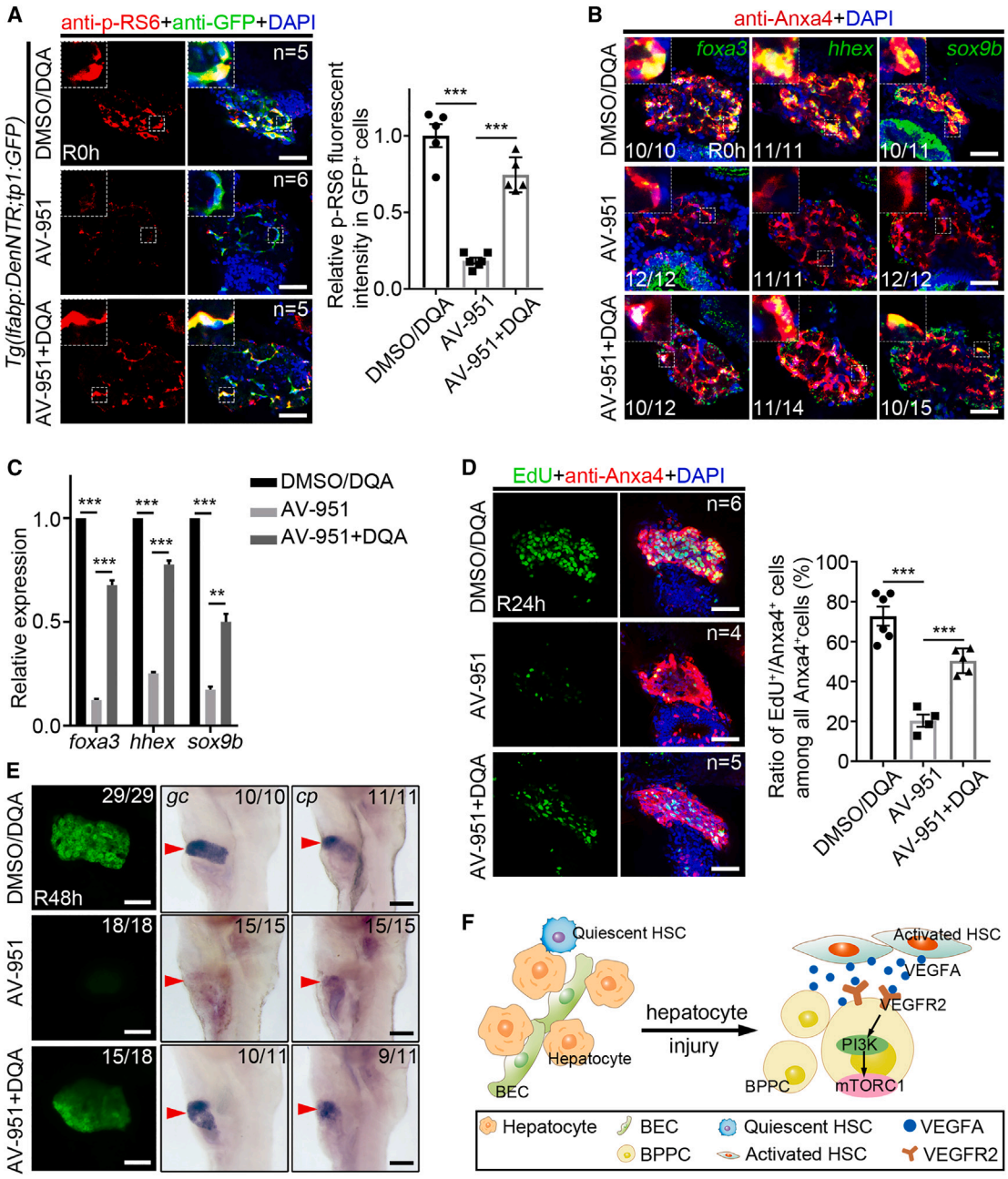

Figure 7. PI3K activation partially rescues defective liver regeneration upon VEGF inhibition

(A) Single-optical section images showing p-RS6 and GFP expression at R0h under *Tg(lfabp:DenNTR;tp1:GFP)* background. Scale bars: 50 μm. The timeline of DQA treatment is consistent with AV-951. Quantification of the relative fluorescent intensity of p-RS6 expression in intrahepatic GFP$^+$ cells. n = 5 (DMSO/DQA), 6 (AV-951), and 5 (AV-951+DQA). Unpaired two-tailed Student's t test. ***p < 0.001. Error bars represent SEM.

(B) FISH and Anxa4 antibody staining showing *foxa3*, *hhex*, and *sox9b* expression in Anxa4$^+$ cells at R0h. Scale bars: 50 μm.

(C) qPCR data showing the relative expression levels of *foxa3*, *hhex*, and *sox9b* at R0h. n = 3 technical replicates. Unpaired two-tailed Student's t test. **p < 0.01, ***p < 0.001. Error bars represent SEM.

(D) Confocal projection images showing EdU staining and Anxa4 antibody staining at R24h. Scale bars: 50 μm. Quantification of the ratio of EdU$^+$/Anxa4$^+$ cells. n = 6 (DMSO/DQA), 4 (AV-951), and 5 (AV-951+DQA). Unpaired two-tailed Student's t test. ***p < 0.001. Error bars represent SEM.

(E) Confocal projection images showing the *lfabp:DenNTR* expression at R48h. Scale bars: 50 μm. WISH images showing *gc* and *cp* expression at R48h. Scale bars: 100 μm.

(F) Illustration summarizing the roles of VEGF signaling in zebrafish liver regeneration.

See also Figures S4–S7.

VEGFR2/Kdrl in BECs after liver injury, and the treatment of VEGFR2-specific inhibitor SU5416 or knockout of *kdrl* led to similar defective phenotypes as the general inhibitor treatment. This phenomenon may be explained by the specific roles of VEGFR2 in PI3K-mTOR activation, which is also found in angiogenesis.[44] The binding of VEGFA to VEGFR2 activates the receptor's kinase activity and stimulates downstream signaling such as PI3K-mTOR.[45] Similarly, extreme-hepatocyte-injury-induced VEGFA expression activates VEGF signaling in BECs through binding to VEGFR2 and subsequently stimulates the PI3K-mTORC1 axis, thus initiating biliary-mediated liver regeneration (Figure 7F). Despite *kdrl* expression being induced in most BECs upon extreme hepatocyte injury, a small portion of BECs exhibited relatively lower expression (Figures 1G and S1C). The difference of *kdrl* expression in each BEC type could be reasoned by the heterogeneity of BECs.[46–48] *kdrl*-expressed BECs may exhibit higher progenitor cell potentiality, and the entire hepatocyte regeneration could be mainly contributed by these cells' transdifferentiation. This hypothesis could be evidenced by a study on human and mouse liver development in which KDR identifies a subset of liver progenitor cells possessing the potential to differentiate into both hepatocytes and cholangiocytes.[49]

In summary, VEGF signaling regulates the early phase of BEC dedifferentiation by activating the PI3K-mTORC1 axis during biliary-mediated liver regeneration. Given the adverse effects of VEGF inhibitors in hepatocyte regeneration and the widespread application of VEGF inhibitors in clinical therapies of multiple cancers including hepatocellular carcinoma, the dosage and duration of medication should be adequately controlled.

Limitations of the study

The scRNA-seq and *in situ* hybridization data both show the upregulation of *vegfaa* in HSCs upon liver injury; however, the question of how *vegfaa* expression is induced remains unknown and needs further investigation. Besides, *kdrl-CreER*-based lineage-tracing experiments could provide evidence for the potential contribution of *kdrl*-expressed biliary cells to the entire liver regeneration. Finally, whether VEGF hyperactivation could promote the generation of biliary-derived hepatocytes and thereby accelerate liver repair remains a crucial inquiry that holds clinical significance for the therapeutics of patients with end-stage liver disease.

STAR★METHODS

Detailed methods are provided in the online version of this paper and include the following:

- KEY RESOURCES TABLE
- RESOURCE AVAILABILITY
  - Lead contact
  - Materials availability
  - Data and code availability
- EXPERIMENTAL MODEL AND SUBJECT PARTICIPANT DETAILS
  - Animal strains
- METHOD DETAILS
  - Generation and genotyping of the *kdrl* mutant
  - Generation of *Tg(hsp70L:dnvegfaa-P2A-DsRed)*, *Tg(krt18:Tet3G;Tre3G:ZsGreen-dnvegfaa-P2A-DsRed)*, and *Tg(krt18:Tet3G;Tre3G:ZsGreen-dnkdrl-P2A-DsRed)*
  - *In situ* hybridization, antibody staining, and imaging
  - Western blotting
  - Chemical treatment
  - 4-Hydroxytamoxifen induced CreER recombination in zebrafish
  - Doxycycline induced Tet-On activation
  - Quantitative real-time PCR (qPCR)
  - Cell sorting
  - 5-Ethynyl-2′-deoxyuridine (EdU) incorporation assay
  - Heat-shock induction
  - Analysis of scRNA-seq data
  - Mouse oval cell activation model
  - Mouse BEC-to-hepatocyte conversion model
  - Antibody staining for mouse liver tissues
- QUANTIFICATION AND STATISTICAL ANALYSIS

SUPPLEMENTAL INFORMATION

Supplemental information can be found online at https://doi.org/10.1016/j.celrep.2023.113028.

ACKNOWLEDGMENTS

We thank Li Nie and Jingying Chen for discussions and technical assistance and Jinrong Peng for the Bhmt antibody. This work was supported by the National Natural Science Foundation of China (32192400 and 32200687), the Natural Science Foundation of Chongqing, China (CSTB2022NSCQ-MSX0481), the National Key R&D Program of China (2021YFA0805000), and the Special fund for youth team of the Southwest University (SWU-XJLJ202302).

AUTHOR CONTRIBUTIONS

L.L., P.C., J.H., and R.N. designed the experimental strategy, analyzed data, and wrote the manuscript. R.N. performed the cell sorting. M.L. generated the *kdrl* mutant and the *dnvegfaa-/dnkdrl*-overexpression lines and performed the WISH experiments. R.N. and H.L. performed the mouse experiments. J.Z. performed the FISH experiments. P.C. performed all other experiments.

DECLARATION OF INTERESTS

The authors declare no competing interests.

Received: March 7, 2023
Revised: July 12, 2023
Accepted: August 10, 2023
Published: August 24, 2023

REFERENCES

1. Zaret, K.S., and Grompe, M. (2008). Generation and Regeneration of Cells of the Liver and Pancreas. Science *322*, 1490–1494. https://doi.org/10.1126/science.1161431.
2. Choi, T.Y., Ninov, N., Stainier, D.Y.R., and Shin, D. (2014). Extensive Conversion of Hepatic Biliary Epithelial Cells to Hepatocytes After Near Total Loss of Hepatocytes in Zebrafish. Gastroenterology *146*, 776–788. https://doi.org/10.1053/j.gastro.2013.10.019.
3. He, J., Lu, H., Zou, Q., and Luo, L. (2014). Regeneration of Liver After Extreme Hepatocyte Loss Occurs Mainly via Biliary Transdifferentiation in Zebrafish. Gastroenterology *146*, 789–800.e8. https://doi.org/10.1053/j.gastro.2013.11.045.

4. Raven, A., Lu, W.Y., Man, T.Y., Ferreiragonzalez, S., Oduibhir, E., Dwyer, B.J., Thomson, J.P., Meehan, R.R., Bogorad, R., Koteliansky, V., et al. (2017). Cholangiocytes act as facultative liver stem cells during impaired hepatocyte regeneration. Nature *547*, 350–354. https://doi.org/10.1038/nature23015.

5. Deng, X., Zhang, X.N., Li, W., Feng, R.X., Li, L., Yi, G.R., Zhang, X., Yin, C., Yu, H.Y., Zhang, J.P., et al. (2018). Chronic Liver Injury Induces Conversion of Biliary Epithelial Cells into Hepatocytes. Cell Stem Cell *23*, 114–122.e3. https://doi.org/10.1016/j.stem.2018.05.022.

6. Sato, K., Marzioni, M., Meng, F., Francis, H., Glaser, S., and Alpini, G. (2019). Ductular Reaction in Liver Diseases: Pathological Mechanisms and Translational Significances. Hepatology *69*, 420–430. https://doi.org/10.1002/hep.30150.

7. Zhou, H., Rogler, L.E., Teperman, L., Morgan, G., and Rogler, C.E. (2007). Identification of hepatocytic and bile ductular cell lineages and candidate stem cells in bipolar ductular reactions in cirrhotic human liver. Hepatology *45*, 716–724. https://doi.org/10.1002/hep.21557.

8. Stueck, A.E., and Wanless, I.R. (2015). Hepatocyte Buds Derived From Progenitor Cells Repopulate Regions of Parenchymal Extinction in Human Cirrhosis. Hepatology *61*, 1696–1707. https://doi.org/10.1002/hep.27706.

9. Goessling, W., and Sadler, K.C. (2015). Zebrafish: An Important Tool for Liver Disease Research. Gastroenterology *149*, 1361–1377. https://doi.org/10.1053/j.gastro.2015.08.034.

10. He, J., Chen, J., Wei, X., Leng, H., Mu, H., Cai, P., and Luo, L. (2019). Mammalian Target of Rapamycin Complex 1 Signaling Is Required for the Dedifferentiation From Biliary Cell to Bipotential Progenitor Cell in Zebrafish Liver Regeneration. Hepatology *70*, 2092–2106. https://doi.org/10.1002/hep.30790.

11. Cai, P., Mao, X., Zhao, J., Nie, L., Jiang, Y., Yang, Q., Ni, R., He, J., and Luo, L. (2021). Farnesoid X Receptor Is Required for the Redifferentiation of Bipotential Progenitor Cells During Biliary-Mediated Zebrafish Liver Regeneration. Hepatology *74*, 3345–3361. https://doi.org/10.1002/hep.32076.

12. Choi, T.Y., Khaliq, M., Tsurusaki, S., Ninov, N., Stainier, D.Y.R., Tanaka, M., and Shin, D. (2017). Bone morphogenetic protein signaling governs biliary-driven liver regeneration in zebrafish through tbx2b and id2a. Hepatology *66*, 1616–1630. https://doi.org/10.1002/hep.29309.

13. Ko, S., Russell, J.O., Tian, J., Gao, C., Kobayashi, M., Feng, R., Yuan, X., Shao, C., Ding, H., and Poddar, M. (2019). Hdac1 Regulates Differentiation of Bipotent Liver Progenitor Cells During Regeneration via Sox9b and Cdk8. Gastroenterology *156*, 187–202.e14. https://doi.org/10.1053/j.gastro.2018.09.039.

14. Zhang, J., Zhou, Y., Li, S., Mo, D., Ma, J., Ni, R., Yang, Q., He, J., and Luo, L. (2022). Tel2 regulates redifferentiation of bipotential progenitor cells via Hhex during zebrafish liver regeneration. Cell Rep. *39*, 110596. https://doi.org/10.1016/j.celrep.2022.110596.

15. He, J., Zhou, Y., Qian, C., Wang, D., Yang, Z., Huang, Z., Sun, J., Ni, R., Yang, Q., Chen, J., and Luo, L. (2022). DNA methylation maintenance at the p53 locus initiates biliary-mediated liver regeneration. NPJ Regen. Med. *7*, 21. https://doi.org/10.1038/s41536-022-00217-8.

16. Simons, M., Gordon, E., and Claesson-Welsh, L. (2016). Mechanisms and regulation of endothelial VEGF receptor signalling. Nat. Rev. Mol. Cell Biol. *17*, 611–625. https://doi.org/10.1038/nrm.2016.87.

17. Apte, R.S., Chen, D.S., and Ferrara, N. (2019). VEGF in Signaling and Disease: Beyond Discovery and Development. Cell *176*, 1248–1264. https://doi.org/10.1016/j.cell.2019.01.021.

18. Cheng, A.-L., Kang, Y.-K., Chen, Z., Tsao, C.-J., Qin, S., Kim, J.S., Luo, R., Feng, J., Ye, S., Yang, T.-S., et al. (2009). Efficacy and safety of sorafenib in patients in the Asia-Pacific region with advanced hepatocellular carcinoma: a phase III randomised, double-blind, placebo-controlled trial. Lancet Oncol. *10*, 25–34. https://doi.org/10.1016/s1470-2045(08)70285-7.

19. Llovet, J.M., Ricci, S., Mazzaferro, V., Hilgard, P., Gane, E., Blanc, J.F., de Oliveira, A.C., Santoro, A., Raoul, J.L., Forner, A., et al. (2008). Sorafenib in advanced hepatocellular carcinoma. N. Engl. J. Med. *359*, 378–390. https://doi.org/10.1056/NEJMoa0708857.

20. Hu, J., Srivastava, K., Wieland, M., Runge, A., Mogler, C., Besemfelder, E., Terhardt, D., Vogel, M.J., Cao, L., Korn, C., et al. (2014). Endothelial Cell-Derived Angiopoietin-2 Controls Liver Regeneration as a Spatiotemporal Rheostat. Science *343*, 416–419. https://doi.org/10.1126/science.1244880.

21. Parsons, M.J., Pisharath, H., Yusuff, S., Moore, J.C., Siekmann, A.F., Lawson, N., and Leach, S.D. (2009). Notch-responsive cells initiate the secondary transition in larval zebrafish pancreas. Mech. Dev. *126*, 898–912. https://doi.org/10.1016/j.mod.2009.07.002.

22. Bruton, F.A., Kaveh, A., Ross-Stewart, K.M., Matrone, G., Oremek, M.E.M., Solomonidis, E.G., Tucker, C.S., Mullins, J.J., Lucas, C.D., Brittan, M., et al. (2022). Macrophages trigger cardiomyocyte proliferation by increasing epicardial vegfaa expression during larval zebrafish heart regeneration. Dev. Cell *57*, 1512–1528.e5. https://doi.org/10.1016/j.devcel.2022.05.014.

23. Tamosiuniene, R., Manouvakhova, O., Mesange, P., Saito, T., Qian, J., Sanyal, M., Lin, Y.-C., Nguyen, L.P., Luria, A., Tu, A.B., et al. (2018). Dominant Role for Regulatory T Cells in Protecting Females Against Pulmonary Hypertension. Circ. Res. *122*, 1689–1702. https://doi.org/10.1161/circresaha.117.312058.

24. Keskin, U., Totan, Y., Karadağ, R., Erdurmuş, M., and Aydın, B. (2012). Inhibitory Effects of SU5416, a Selective Vascular Endothelial Growth Factor Receptor Tyrosine Kinase Inhibitor, on Experimental Corneal Neovascularization. Ophthalmic Res. *47*, 13–18. https://doi.org/10.1159/000324994.

25. Jin, D., Zhu, D., Fang, Y., Chen, Y., Yu, G., Pan, W., Liu, D., Li, F., and Zhong, T.P. (2017). Vegfa signaling regulates diverse artery/vein formation in vertebrate vasculatures. J. Genet. Genomics *44*, 483–492. https://doi.org/10.1016/j.jgg.2017.07.005.

26. Marín-Juez, R., Marass, M., Gauvrit, S., Rossi, A., Lai, S.-L., Materna, S.C., Black, B.L., and Stainier, D.Y.R. (2016). Fast revascularization of the injured area is essential to support zebrafish heart regeneration. Proc. Natl. Acad. Sci. USA *113*, 11237–11242. https://doi.org/10.1073/pnas.1605431113.

27. Mitra, S., Devi, S., Lee, M.-S., Jui, J., Sahu, A., and Goldman, D. (2022). Vegf signaling between Muller glia and vascular endothelial cells is regulated by immune cells and stimulates retina regeneration. Proc. Natl. Acad. Sci. USA *119*, e2211690119. https://doi.org/10.1073/pnas.2211690119.

28. Rossi, A., Gauvrit, S., Marass, M., Pan, L., Moens, C.B., and Stainier, D.Y.R. (2016). Regulation of Vegf signaling by natural and synthetic ligands. Blood *128*, 2359–2366. https://doi.org/10.1182/blood-2016-04-711192.

29. Covassin, L.D., Villefranc, J.A., Kacergis, M.C., Weinstein, B.M., and Lawson, N.D. (2006). Distinct genetic interactions between multiple Vegf receptors are required for development of different blood vessel types in zebrafish. Proc. Natl. Acad. Sci. USA *103*, 6554–6559. https://doi.org/10.1073/pnas.0506886103.

30. Zhang, C., Ellis, J.L., and Yin, C. (2016). Inhibition of vascular endothelial growth factor signaling facilitates liver repair from acute ethanol-induced injury in zebrafish. Dis. Model. Mech. *9*, 1383–1396. https://doi.org/10.1242/dmm.024950.

31. Saxton, R.A., and Sabatini, D.M. (2017). mTOR Signaling in Growth, Metabolism, and Disease. Cell *168*, 960–976. https://doi.org/10.1016/j.cell.2017.02.004.

32. Xiao, H.-b., Cao, X., Wang, L., Run, X.-q., Su, Y., Tian, C., Sun, S.-g., and Liang, Z.-h. (2011). 1,5-dicaffeoylquinic acid protects primary neurons from amyloid beta(1-42)-induced apoptosis via PI3K/Akt signaling pathway. Chin. Med. J. *124*, 2628–2635. https://doi.org/10.3760/cma.j.issn.0366-6999.2011.17.012.

33. Sakurai, M., Ishitsuka, K., Ito, R., Wilkinson, A.C., Kimura, T., Mizutani, E., Nishikii, H., Sudo, K., Becker, H.J., Takemoto, H., et al. (2023). Chemically

defined cytokine-free expansion of human haematopoietic stem cells. Nature *615*, 127–133. https://doi.org/10.1038/s41586-023-05739-9.

34. Ko, S., Choi, T.-Y., Russell, J.O., So, J., Monga, S.P.S., and Shin, D. (2016). Bromodomain and extraterminal (BET) proteins regulate biliary-driven liver regeneration. J. Hepatol. *64*, 316–325. https://doi.org/10.1016/j.jhep.2015.10.017.
35. Español-Suñer, R., Carpentier, R., Van Hul, N., Legry, V., Achouri, Y., Cordi, S., Jacquemin, P., Lemaigre, F., and Leclercq, I.A. (2012). Liver Progenitor Cells Yield Functional Hepatocytes in Response to Chronic Liver Injury in Mice. Gastroenterology *143*, 1564–1575.e7. https://doi.org/10.1053/j.gastro.2012.08.024.
36. Russell, J.O., Lu, W.-Y., Okabe, H., Abrams, M., Oertel, M., Poddar, M., Singh, S., Forbes, S.J., and Monga, S.P. (2019). Hepatocyte-Specific beta-Catenin Deletion During Severe Liver Injury Provokes Cholangiocytes to Differentiate Into Hepatocytes. Hepatology *69*, 742–759. https://doi.org/10.1002/hep.30270.
37. Gaudio, E., Barbaro, B., Alvaro, D., Glaser, S., Francis, H., Ueno, Y., Meininger, C.J., Franchitto, A., Onori, P., Marzioni, M., et al. (2006). Vascular endothelial growth factor stimulates rat cholangiocyte proliferation via an autocrine mechanism. Gastroenterology *130*, 1270–1282. https://doi.org/10.1053/j.gastro.2005.12.034.
38. Glaser, S., Meng, F., Han, Y., Onori, P., Chow, B.K., Francis, H., Venter, J., McDaniel, K., Marzioni, M., Invernizzi, P., et al. (2014). Secretin Stimulates Biliary Cell Proliferation by Regulating Expression of MicroRNA 125b and MicroRNA let7a in Mice. Gastroenterology *146*, 1795–1808.e12. https://doi.org/10.1053/j.gastro.2014.02.030.
39. Ankoma-Sey, V., Wang, Y., and Dai, Z. (2000). Hypoxic stimulation of vascular endothelial growth factor expression in activated rat hepatic stellate cells. Hepatology *31*, 141–148. https://doi.org/10.1002/hep.510310122.
40. Yoshiji, H., Kuriyama, S., Yoshii, J., Ikenaka, Y., Noguchi, R., Hicklin, D.J., Wu, Y., Yanase, K., Namisaki, T., Yamazaki, M., et al. (2003). Vascular endothelial growth factor and receptor interaction is a prerequisite for murine hepatic fibrogenesis. Gut *52*, 1347–1354. https://doi.org/10.1136/gut.52.9.1347.
41. Sahin, H., Borkham-Kamphorst, E., Kuppe, C., Zaldivar, M.M., Grouls, C., Al-samman, M., Nellen, A., Schmitz, P., Heinrichs, D., Berres, M.-L., et al. (2012). Chemokine Cxcl9 attenuates liver fibrosis-associated angiogenesis in mice. Hepatology *55*, 1610–1619. https://doi.org/10.1002/hep.25545.
42. Yang, L., Kwon, J., Popov, Y., Gajdos, G.B., Ordog, T., Brekken, R.A., Mukhopadhyay, D., Schuppan, D., Bi, Y., Simonetto, D., and Shah, V.H. (2014). Vascular Endothelial Growth Factor Promotes Fibrosis Resolution and Repair in Mice. Gastroenterology *146*, 1339–1350.e1. https://doi.org/10.1053/j.gastro.2014.01.061.
43. Yin, C., Evason, K.J., Maher, J.J., and Stainier, D.Y.R. (2012). The basic helix-loop-helix transcription factor, heart and neural crest derivatives expressed transcript 2, marks hepatic stellate cells in zebrafish: Analysis of stellate cell entry into the developing liver. Hepatology *56*, 1958–1970. https://doi.org/10.1002/hep.25757.
44. Zhang, P.-C., Liu, X., Li, M.M., Ma, Y.-Y., Sun, H.-T., Tian, X.-Y., Wang, Y., Liu, M., Fu, L.-S., Wang, Y.-F., et al. (2020). AT-533, a novel Hsp90 inhibitor, inhibits breast cancer growth and HIF-1 alpha/VEGF/VEGFR-2-mediated angiogenesis in vitro and in vivo. Biochem. Pharmacol. *172*, 113771. https://doi.org/10.1016/j.bcp.2019.113771.
45. Ruan, G.-X., and Kazlauskas, A. (2012). Axl is essential for VEGF-A-dependent activation of PI3K/Akt. EMBO J. *31*, 1692–1703. https://doi.org/10.1038/emboj.2012.21.
46. Pu, W., Zhu, H., Zhang, M., Pikiolek, M., Ercan, C., Li, J., Huang, X., Han, X., Zhang, Z., Lv, Z., et al. (2023). Bipotent transitional liver progenitor cells contribute to liver regeneration. Nat. Genet. *55*, 651–664. https://doi.org/10.1038/s41588-023-01335-9.
47. Aizarani, N., Saviano, A., Sagar, L., Mailly, L., Durand, S., Herman, J.S., Pessaux, P., Baumert, T.F., and Grün, D. (2019). A human liver cell atlas reveals heterogeneity and epithelial progenitors. Nature *572*, 199–204. https://doi.org/10.1038/s41586-019-1373-2.
48. Pepe-Mooney, B.J., Dill, M.T., Alemany, A., Ordovas-Montanes, J., Matsushita, Y., Rao, A., Sen, A., Miyazaki, M., Anakk, S., Dawson, P.A., et al. (2019). Single-Cell Analysis of the Liver Epithelium Reveals Dynamic Heterogeneity and an Essential Role for YAP in Homeostasis and Regeneration. Cell Stem Cell *25*, 23–38.e8. https://doi.org/10.1016/j.stem.2019.04.004.
49. Goldman, O., Han, S., Sourisseau, M., Dziedzic, N., Hamou, W., Corneo, B., D'Souza, S., Sato, T., Kotton, D.N., Bissig, K.-D., et al. (2013). KDR Identifies a Conserved Human and Murine Hepatic Progenitor and Instructs Early Liver Development. Cell Stem Cell *12*, 748–760. https://doi.org/10.1016/j.stem.2013.04.026.
50. Chang, N., Sun, C., Gao, L., Zhu, D., Xu, X., Zhu, X., Xiong, J.W., and Xi, J.J. (2013). Genome editing with RNA-guided Cas9 nuclease in zebrafish embryos. Cell Res. *23*, 465–472. https://doi.org/10.1038/cr.2013.45.
51. Sun, J., Chen, Q., and Ma, J. (2022). Notch-Sox9 Axis Mediates Hepatocyte Dedifferentiation in Kras(G12V)-Induced Zebrafish Hepatocellular Carcinoma. Int. J. Mol. Sci. *23*, 4705. https://doi.org/10.3390/ijms23094705.
52. Chen, J., He, J., Ni, R., Yang, Q., Zhang, Y., and Luo, L. (2019). Cerebrovascular Injuries Induce Lymphatic Invasion into Brain Parenchyma to Guide Vascular Regeneration in Zebrafish. Dev. Cell *49*, 697–710.e5. https://doi.org/10.1016/j.devcel.2019.03.022.
53. Lu, H., Ma, J., Yang, Y., Shi, W., and Luo, L. (2013). EpCAM is an endoderm-specific Wnt derepressor that licenses hepatic development. Dev. Cell *24*, 543–553. https://doi.org/10.1016/j.devcel.2013.01.021.
54. He, J., Mo, D., Chen, J., and Luo, L. (2020). Combined whole-mount fluorescence in situ hybridization and antibody staining in zebrafish embryos and larvae. Nat. Protoc. *15*, 3361–3379. https://doi.org/10.1038/s41596-020-0376-7.
55. Liu, C., Wu, C., Yang, Q., Gao, J., Li, L., Yang, D., and Luo, L. (2016). Macrophages Mediate the Repair of Brain Vascular Rupture through Direct Physical Adhesion and Mechanical Traction. Immunity *44*, 1162–1176. https://doi.org/10.1016/j.immuni.2016.03.008.
56. Cao, Z., Mao, X., and Luo, L. (2019). Germline Stem Cells Drive Ovary Regeneration in Zebrafish. Cell Rep. *26*, 1709–1717.e3. https://doi.org/10.1016/j.celrep.2019.01.061.
57. Yang, Y., Li, Y., Fu, J., Li, Y., Li, S., Ni, R., Yang, Q., and Luo, L. (2022). Intestinal precursors avoid being misinduced to liver cells by activating Cdx-Wnt inhibition cascade. Proc. Natl. Acad. Sci. USA *119*, e2205110119. https://doi.org/10.1073/pnas.2205110119.

STAR★METHODS

KEY RESOURCES TABLE

REAGENT or RESOURCE	SOURCE	IDENTIFIER
Antibodies		
Rabbit anti-Dendra2 (1:1000)	Evrogen	Cat#AB821
Goat anti-GFP (1:1000)	Abcam	Cat#ab6658; RRID:AB_305631
Rabbit anti-GFP (1:500)	Invitrogen	Cat#A-11122; RRID:AB_221569
Mouse anti-Bhmt (1:500)	A gift from J. Peng, Zhejiang University, China	N/A
Goat anti-Hnf4α (1:50)	Santa Cruz	Cat#SC6556; RRID:AB_2117025
Mouse anti-Anxa4 (1:500)	Abcam	Cat#ab71286; RRID:AB_1209226
Rabbit anti-p-RS6 (1:500)	Cell Signaling	Cat#2215; RRID:AB_331682
Rabbit anti-p-Vegfr2 (Tyr1175) (1:1000)	Affinity	Cat#AF4426; RRID:AB_2844490
Goat anti-mCherry or anti-DsRed (1:500)	Arigo biolaboratories	Cat#ARG55723
Rabbit anti-CK19 (1:500)	Abcam	Cat#ab133496; RRID:AB_11155282
Rabbit anti-Sox9 (1:500)	Merck Millipore	Cat#AB5535; RRID:AB_2239761
Rabbit anti-Ki67 (1:200)	Invitrogen	Cat#PA5-16785; RRID:AB_11000602
Rabbit anti-Ctnnb1 (1:200)	Abcam	Cat#ab32572; RRID:AB_725966
Anti-digoxigenin POD, Fab fragment	Roche	Cat#11207733910; RRID:AB_514500
Anti-digoxigenin AP, Fab fragment	Roche	Cat#11093274910; RRID:AB_514497
Donkey anti-goat IgG Alexa fluor 633-conjugated (1:1000)	Invitrogen	Cat#A21082; RRID:AB_2535739
Donkey anti-mouse IgG Alexa fluor 568-conjugated (1:1000)	Invitrogen	Cat#A10037; RRID:AB_2534013
Donkey anti-mouse IgG Alexa fluor 647-conjugated (1:1000)	Invitrogen	Cat#A31571; RRID:AB_162542
Donkey anti-rabbit IgG Alexa fluor 647-conjugated (1:1000)	Invitrogen	Cat#A31573; RRID:AB_2536183
Donkey anti-rabbit IgG Alexa fluor 488-conjugated (1:1000)	Invitrogen	Cat#A21206; RRID:AB_2535792
Chemicals, peptides, and recombinant proteins		
1-phenyl-2-thiourea (PTU)	Sigma-Aldrich	Cat#P7629
SU5416	Aladdin	Cat#S125835
AV-951	Glpbio	Cat#GC12036
LY294002	Aladdin	Cat#L124970
1,3-*O*-Dicaffeoylquinic acid	Glpbio	Cat#GC35037
4-Hydroxytamoxifen	Sigma	Cat#H7904
Tamoxifen	Sigma	Cat#T5648
740 Y-P	Selleck	Cat#S7865
Metronidazole	Sigma-Aldrich	Cat#M3761
Rapamycin	Selleck	Cat#AY-22989
Ethionine	Aladdin	Cat#E117217
Blocking reagent	Roche	Cat#11096176001
SuperSignal West Pico Chemiluminescent Substrate	Thermo Fisher Scientific	Cat#34577
NBT/BCIP stock solution	Roche	Cat#11681451001
Quick Antigen Retrieval Solution for Frozen Sections	Beyotime	Cat#P0090
Tripure isolation reagent	Roche	Cat#11667165001

(*Continued on next page*)

Continued

REAGENT or RESOURCE	SOURCE	IDENTIFIER
Critical commercial assays		
TSA Plus Cy5 Fluorescence System	Perkin Elmer	Cat#NEL745
Omniscript RT Kit	Qiagen	Cat#205110
FastStart Universal SYBR Green Master	Roche	Cat#04913914001
Click-iT EdU Alexa Fluor 647 Kit	Invitrogen	Cat#C10340
Deposited data		
Raw scRNA-seq data	This study	SRA: PRJNA975724
Experimental models: Organisms/strains		
Zebrafish: *Tg(lfabp:Dendra2-NTR)^{cq1}* abbreviated as *Tg(lfabp:DenNTR)*	He et al.[3]	ZFIN: ZDB-TGCONSTRCT-150922-2
Zebrafish: *Tg(tp1bglob:EGFP)^{um14}* abbreviated as *Tg(tp1:GFP)*	Parsons et al.[21]	ZFIN: ZDB-TGCONSTRCT-090625-1
Zebrafish: *Tg(lfabp:CFP-NTR)^{s931}*	Choi et al.[2]	ZFIN: ZDB-TGCONSTRCT-070710-2
Zebrafish: *TgBAC(hand2:GFP)^{cq106}* abbreviated as *Tg(hand2:GFP)*	Cai et al.[11]	N/A
Zebrafish: *Tg(krt18:CreERT2)^{cq74}* abbreviated as *Tg(krt18:CreER)*	He et al.[10]	ZFIN: ZDB-TGCONSTRCT-211105-2
Zebrafish: *Tg(lfabp:loxP-STOP-loxP-DsRed)^{cq4}* abbreviated as *Tg(lfabp:LSL-DsRed)*	He et al.[10]	ZFIN: ZDB-ALT-150922-6
Zebrafish:*Tg(krt18:Tet3G)^{cq134}*	He et al.[15]	N/A
Zebrafish: *Tg(hsp70L:dnvegfaa-P2A-DsRed)^{cq176}* abbreviated as *Tg(hsp:dnvegfaa)*	This study	N/A
Zebrafish:*Tg(Tre3G:ZsGreen-dnvegfaa-P2A-DsRed)^{cq177}*	This study	N/A
Zebrafish:*Tg(Tre3G:ZsGreen-dnkdrl-P2A-DsRed)^{cq178}*	This study	N/A
Zebrafish: *kdrl mutant^{cq179}*	This study	N/A
Mouse: C57BL/6J	GemPharmatech	N/A
Mouse: *Ctnnb1$^{flox/flox}$*	Jackson Laboratory	Cat#004152
Mouse: *Rosa-stop$^{flox/flox}$-tdTomato* abbreviated as *tdTomato^{LSL}*	Biocytogen	N/A
Mouse: *Osteopontin-CreERT2-IRES-EGFP* abbreviated as *OPN-CreER*	GemPharmatech	Cat#T049832
Oligonucleotides		
Primers for *kdrl* mutant genotyping: Forward: 5′-ATGTCAATCAAAATCACCTGAACT-3′ Reverse: 5′-GCTGGACTTCTTGTGACTGC-3′	Beijing Genomics institution (BGI)	N/A
Primers for *dnvegfaa* (F17A) mutagenesis: Forward: 5′-AATGATGTGATTCCCGCTA TGGATGTGTATAAA-3′ Reverse: 5′-TTTATACACATCCATAGCG GGAATCACATCATT-3′	BGI	N/A
Primers for *dnvegfaa* (K84A) mutagenesis: Forward: 5′-GGTGCTGCGGGTCGCGC AACGCGTATCGC-3′ Reverse: 5′-GCGATACGCGTTGCGCG ACCCGCAGCACC-3′	BGI	N/A
Primers for *P2A-DsRed* fragment cloning: Forward: 5′-TCGCAGCATAATTTTCAG CGGAAGCGGAGCTACTAACTTC-3′ Reverse: 5′-CTACAGGAACAGGTGGTGGC-3′	BGI	N/A
Primers for *dnkdrl* fragment cloning: Forward: 5′-ATGACTCCTCTTAAAACCTC-3′ Reverse: 5′-TCAATGGCCCAAAGTTTTACCG-3′	BGI	N/A

(*Continued on next page*)

Continued

REAGENT or RESOURCE	SOURCE	IDENTIFIER
qPCR primers, *vegfaa* Forward: 5′-GAGATCGAGCACACGTACATC-3′ Reverse: 5′-CACCTCCATAGTGACGTTTCG-3′	BGI	N/A
qPCR primers, *eef1a1l1* Forward: 5′-CTGGAGGCCAGCTCAAACAT-3′ Reverse: 5′-ATCAAGAAGAGTAGTAC CGCTAGCATTAC-3′	BGI	N/A
qPCR primers, *foxa3* Forward: 5′-TGAAATTCCGGAGTGGAATC-3′ Reverse: 5′-GCTGGGATAGCCCATATTCA-3′	BGI	N/A
qPCR primers, *hhex* Forward: 5′-CCGAACTCCTCTTTCACCAGCCT-3′ Reverse: 5′-GGACGCGTACTGGGACAGAACC-3′	BGI	N/A
qPCR primers, *sox9b* Forward: 5′-CAGAAACACCCGACTCCAG-3′ Reverse: 5′-CACACCGGCAGATCTGTTT-3′	BGI	N/A
qPCR primers, *kdrl* Forward: 5′-ACGGAGTATCATTCGGGACG-3′ Reverse: 5′-TCCCTCTACCAAACCATGTGAA-3′	BGI	N/A
qPCR primers, *cp* Forward: 5′-CAGCACACTTCCACGGCCAC-3′ Reverse: 5′-GGTCGGTCACATGACAGTGC-3′	BGI	N/A
qPCR primers, *gc* Forward: 5′-GCTCGCAGTACTCCAAACTGG-3′ Reverse: 5′-ACAGTTGTGCCGGTGAGAGC-3′	BGI	N/A
qPCR primers, *tfa* Forward: 5′-GTTGATGGTGGCCAGGTGTA-3′ Reverse: 5′-GTAACTTGCGGTCCCTCCTG-3′	BGI	N/A
qPCR primers, *hnf4a* Forward: 5′-GCCGACACTACAGAGCATCA-3′ Reverse: 5′-TGGTAGGTTGAGGGATGGAG-3′	BGI	N/A
qPCR primers, *vegfab* Forward: 5′-CCAGGGTGGCTCAAAAATTAGTC-3′ Reverse: 5′-AGTGTTTGCAGGAGCACTGA-3′	BGI	N/A
qPCR primers, *vegfba* Forward: 5′-TGGGGATCAAGCTGAGGGTT-3′ Reverse: 5′-GCATCCAGTGGTCTGACTGT-3′	BGI	N/A
qPCR primers, *vegfbb* Forward: 5′-CCACAGATTCGGAGGGGAAT-3′ Reverse: 5′-ACTAGTCTCTGAACCTGCACTG-3′	BGI	N/A
qPCR primers, *vegfc* Forward: 5′-CAAGCAGATGCCATGCAGGA-3′ Reverse: 5′-CCCATCTTGGAACGGCACTT-3′	BGI	N/A
qPCR primers, *vegfd* Forward: 5′-AGGCACAGGAAAAACAGTTG -3′ Reverse: 5′-GATAGCAGACGGCGGTTCTT-3′	BGI	N/A
qPCR primers, *flt1* Forward: 5′-ACACGTTACAGGGCGAGAT -3′ Reverse: 5′-TGGCGGATCCATTAGCCTTC-3′	BGI	N/A
qPCR primers, *flt4* Forward: 5′-GCCAGTGTGCCAGCTATGTA-3′ Reverse: 5′-CGAATCCTTCAGGGATAGTGGT-3′	BGI	N/A
Primers for *vegfaa* probe synthesis: Forward: 5′-GCAACACTCCACTGGAATTAC-3′ Reverse: 5′-TAATACGACTCACTATAGGGCA TCATCTTGGCTTTTCAC-3′	BGI	N/A

(*Continued on next page*)

Continued

REAGENT or RESOURCE	SOURCE	IDENTIFIER
Primers for *foxa3* probe synthesis: Forward: 5′-ATGTTGAGCTCCGTGAAGATG-3′ Reverse: 5′-TAATACGACTCACTATAGGGTTA GGATGCATTGAGGACAGAC-3′	BGI	N/A
Primers for *hhex* probe synthesis: Forward: 5′-ATGCAATTCCAGCACCCGCA-3′ Reverse: 5′-TAATACGACTCACTATAGGGTC ATAGGGTGAACTGATGCTC-3′	BGI	N/A
Primers for *sox9b* probe synthesis: Forward: 5′-ATGAATCTCCTCCAGCGCG-3′ Reverse: 5′-TAATACGACTCACTATAGGGT CAGGGTCTGGACAGCTGT-3′	BGI	N/A
Primers for *kdrl* probe synthesis: Forward: 5′-GATTTGCGATTTTGGACTTGC-3′ Reverse: 5′-TAATACGACTCACTATAGGGC GCTCGGGACATGAAACTC-3′	BGI	N/A
Primers for *cp* probe synthesis: Forward: 5′-GATCTGAGACAGACATCCAC-3′ Reverse: 5′-TAATACGACTCACTATAGGGC AGGTTGCCGAAGACTAAAC-3′	BGI	N/A
Primers for *gc* probe synthesis: Forward: 5′-GCTTTAATAGTCCCAGCATTGC-3′ Reverse: 5′-TAATACGACTCACTATAGGGC CTTAAGCAGCACTGTCATC-3′	BGI	N/A
Primers for *tfa* probe synthesis: Forward: 5′-GAGAAAATCAAGCGCAAAGAAGC-3′ Reverse: 5′-TAATACGACTCACTATAGGGAG CCCCATCATAGCCATAATACTG-3′	BGI	N/A
Primers for *hnf4a* probe synthesis: Forward: 5′-GAATGCGTTTGTCCAAACCAC-3′ Reverse: 5′-TAATACGACTCACTATAGGGCA GATGGCCTCTTGTTTAGTG-3′	BGI	N/A
Primers for *flt1* probe synthesis: Forward: 5′-CGCCATTATCAGCAAACGCA-3′ Reverse: 5′-ATTTAGGTGACACTATAGAA CCTGCAAAAGCCTGAACGAC-3′	BGI	N/A
Primers for *kdr* probe synthesis: Forward: 5′-GCATGGAGTTTCTGGCCTCT-3′ Reverse: 5′-ATTTAGGTGACACTATAGAA CGGACCTCTGCACTGAACTT-3′	BGI	N/A
Primers for *flt4* probe synthesis: Forward: 5′-GTTTGCTGGCTGTGTGATGG-3′ Reverse: 5′-ATTTAGGTGACACTATAGAA TTACAGGTTGGAGGTTGCCG-3′	BGI	N/A
Recombinant DNA		
pBluescript-hsp70L:dnvegfaa-P2A-DsRed	This study	N/A
pBluescript-Tre3G:ZsGreen-dnvegfaa-P2A-DsRed	This study	N/A
pBluescript-Tre3G:ZsGreen-dnkdrl-P2A-DsRed	This study	N/A
Software and algorithms		
ZEN2010 Imaging software	Carl Zeiss	https://www.zeiss.com
Graphpad Prism	Graphpad	https://www.graphpad.com
Adobe Photoshop	Adobe	https://www.adobe.com
Loupe Browser	10x Genomics	www.10xgenomics.com
ImageJ	National Institutes of Health	https://imagej.en.softonic.com

RESOURCE AVAILABILITY

Lead contact

Further information and requests for reagents may be directed to and will be fulfilled by the Lead Contact, Lingfei Luo (lluo@swu.edu.cn).

Materials availability

This study did not generate new unique reagents. All zebrafish lines and plasmids generated in this study are available from the lead contact on request.

Data and code availability

- The data of scRNA-seq in this study have been deposited at the National Center for Biotechnology Information (NCBI) Sequence Read Archive (SRA), https://www.ncbi.nlm.nih.gov/sra (BioProject: PRJNA975724).
- This paper does not report original code.
- Any additional information required to reanalyze the data reported in this paper is available from the lead contact on request.

EXPERIMENTAL MODEL AND SUBJECT PARTICIPANT DETAILS

Animal strains

All experimental procedures were performed according to the standard guidelines and approved by Southwest University (Chongqing, China). Zebrafish and mouse were maintained according to the Guidelines of Experimental Animal Welfare from the Ministry of Science and Technology of China (2006) and the Institutional Animal Care and Use Committee protocols from Southwest University (2007). To inhibit pigmentation, embryos were treated with 0.003% 1-phenyl-2-thiourea from 24 h postfertilization. The full information of all zebrafish strains and mouse lines is provided in the key resource table.

METHOD DETAILS

Generation and genotyping of the *kdrl* mutant

The *kdrl* mutant was generated by targeting the third exon of *kdrl* with CRISPR/Cas9 system.[50] The *kdrl* target sequence was depicted in Figure S3. In brief, 200 ng/μL gRNA and 300 ng/μL Cas9 mRNA were co-injected into 1-cell stage embryos to generate the founder (F0), and then the lysate of 20–30 F0 embryos at 48 hpf was used as templates for PCR. DNA sequencing was performed to determine the efficiency of genome editing. F0 adults with effective genome editing were outcrossed with wild-type fish to get the candidate progeny (F1). F1 heterozygous mutants were screened by sequencing using the tail fin genomic DNA. The primers for genotyping are listed in the key resource table.

Generation of *Tg(hsp70L:dnvegfaa-P2A-DsRed)*, *Tg(krt18:Tet3G;Tre3G:ZsGreen-dnvegfaa-P2A-DsRed)*, and *Tg(krt18:Tet3G;Tre3G:ZsGreen-dnkdrl-P2A-DsRed)*

Zebrafish *dnvegfaa* (F17A/K84A) cds fragment was cloned by site-directed mutagenesis.[26,28] The *P2A-DsRed* fragment was cloned from *hsp70l-mapk3-P2A-DsRed*.[11] The *dnvegfaa-P2A-DsRed* fragment was cloned from *dnvegfaa* cds fragment and *P2A-DsRed* fragment by overlap PCR. Then *pBluescript-hsp70L:dnvegfaa-P2A-DsRed* was generated by replacing the *mapk3-P2A-DsRed* in plasmid *pBluescript-hsp70l-mapk3-P2A-DsRed* with *dnvegfaa-P2A-DsRed*. *pBluescript-hsp70l-dnvegfaa-P2A-DsRed* flanked by the I-SceI restriction sites was co-injected with I-SceI into embryos at the one-cell stage for transgenesis.

Tre3G:ZsGreen-dnvegfaa-P2A-DsRed was generated by replacing the $kras^{G12V}$ in plasmid *TRE3G: ZsGreen-*$kras^{G12V}$.[51] The transgenesis of *Tre3G:ZsGreen-dnvegfaa-P2A-DsRed* is similar to the *hsp70l-dnvegfaa-P2A-DsRed.* Then *Tg(Tre3G:ZsGreen-dnvegfaa-P2A-DsRed)* adults were crossed with *Tg(krt18:Tet3G).*

Zebrafish *dnkdrl* cds fragment was cloned from 24 hpf cDNA. The *dnkdrl-P2A-DsRed* fragment was cloned similar to *dnvegfaa-P2A-DsRed*. Then *Tre3G:ZsGreen-dnkdrl-P2A-DsRed* was generated by replacing the *dnvegfaa-P2A-DsRed* with *dnkdrl-P2A-DsRed* fragment.

In situ hybridization, antibody staining, and imaging

Whole-mount *in situ* hybridization (WISH) and fluorescent *in situ* hybridization (FISH) were performed according to the published protocols.[52–55] The primers used for probe synthesis are listed in the key resource table. Images of WISH were captured using a SteREO DiscoveryV20 microscope equipped with AxioVision Rel 4.8.2 software (Carl Zeiss).

For whole-mount antibody staining, embryos were fixed with 4% PFA at 4°C overnight, and then washed with PBS for 3 times. The skins of embryos were removed using tweezers under a dissecting microscope. Then embryos were washed with 1% PT (1% Triton X-100 in PBS) for 3 times, and then incubated with blocking solution PBTN (1% Triton X-100, 4% BSA, and 0.02% NaN_3 in PBS) at 4°C for 2 h. Embryos were incubated with the primary antibodies (diluted in PBTN) at 4°C overnight. Subsequently, embryos were

washed with PT for 5 times and then incubated with the secondary antibodies (diluted in PBTN) at room temperature for 2 h. At last, embryos were washed with PT for 5 times to minimize the background signals. The full information of primary and secondary antibodies are listed in the key resource table. Images of antibody staining and FISH were captured using ZEN2010 software equipped on an LSM780 or LSM880 confocal microscope (Carl Zeiss).

Western blotting

Total protein lysates were extracted on ice with RIPA buffer (20 mM Tris-HCl, pH 7.5, 150 mM NaCl, 5 mM $MgCl_2$, 1 mM DTT, 0.1% SDS, 1% Triton X-100, 1% sodium deoxycholate, and 10% glycerol, 1× cocktail, 1 mM PMSF, 10 mM sodium fluoride, and 1 mM sodium orthovanadate). The proteins were separated on 10% polyacrylamide gels (Bio-Rad) and transferred to a PVDF membrane. Then the membrane was blocked with 5% BSA and incubated with primary antibodies at 4°C overnight. Then the membrane was washed 5 times with TBST and incubated with appropriate horseradish peroxidase-conjugated secondary antibodies for 1 h at room temperature. SuperSignal West Pico Chemiluminescent Substrate was used to visualize the protein expression levels.

Chemical treatment

To totally ablate hepatocytes, the *Tg(lfabp:DenNTR)* or *Tg(lfabp:CFP-NTR)* transgenic larvae were incubated with 10 mM Mtz for 24 h. To inhibit VEGFR, the larvae were treated with 2 μM SU5416 or 20 nM AV-951. 10 μM LY294002 was used to inhibit PI3K signaling, and 5 μM 1,3-dicaffeoylquinic acid or 5 μM 740 Y-P were used to activate PI3K signaling. 2 μM rapamycin was used to inhibit mTORC1 signaling. We renewed the chemical solutions every 24 h to maintain the pharmacological effects, and a 0.2% DMSO solution in egg water was used as the control.

4-Hydroxytamoxifen induced CreER recombination in zebrafish

To induce CreER activity, 4 dpf *Tg(krt18:CreERT2;lfabp:loxP-STOP-loxP-DsRed; lfabp:DenNTR)* larvae were incubated with 2.5 μM 4-hydroxytamoxifen (4-OHT) for 24 h for the labeling of BEC-derived hepatocytes.

Doxycycline induced Tet-On activation

For the *Tg(krt18:Tet3G;Tre3G:dnvegfaa-P2A-DsRed)* and *Tg(krt18:Tet3G;Tre3G:dnkdrl-P2A-DsRed)* fish, the embryos were treated with 40 μg/mL doxycycline (Dox) from 4 dpf to R48h for the BEC-specific overexpression of *dnvegfaa* or *dnkdrl*.

Quantitative real-time PCR (qPCR)

Total RNA was extracted from dissected livers using Tripure isolation reagent. All liver tissues were manually dissected from the larvae with *Tg(lfabp:DenNTR)* background at R0h and R48h. cDNA was synthesized using Omniscript RT Kit according to the manufacturer's protocol. qPCR was performed using the FastStart Universal SYBR Green Master,[56] normalized by the expression of *eef1a1l1*. The primers used for qPCR are listed in the key resource table.

Cell sorting

The liver tissues of *Tg(tp1:GFP)* or *Tg(hand2:GFP)* larvae were manually dissected at 6 dpf and R0h, then the cells of liver were dissociated and sorted by flow cytometry (Moflo XDP, Beckman).[55] The GFP^+ cells were collected in PBS and then suffered from mRNA extraction with Tripure isolation reagent.

5-Ethynyl-2′-deoxyuridine (EdU) incorporation assay

The EdU assay was applied for S-phase labeling according to the manufacturer's instructions. In brief, the larvae were incubated with 100 μM EdU for 3 h, and then fixed with 4% PFA at 4°C overnight. The samples were washed with PBS for three times, and then the skins were removed manually. Then those larvae were subjected to EdU staining solution.

Heat-shock induction

The larvae of *Tg(lfabp:DenNTR; hsp:dnvegfaa)* were heat-shocked at 38.5°C for 40 min and then incubated at 28.5°C, and the heat-shock was performed every 12 h from 5 dpf to R48h.

Analysis of scRNA-seq data

The RNA sequencing were performed by the AccuraMed Company (Shanghai, China). Single-cell RNA-seq was performed by droplet-based sequencing (10x Genomics).[57] The images of UMAP plot were generated using the Loupe Browser (version 5.0.1).

Mouse oval cell activation model

To induce liver injury, 2-month-old C57BL/6J mice were given a choline-deficient diet (Xietong Biotech, Nanjing, China) supplemented with 0.15% ethionine drinking water for 14 days. 10 mg/kg AV-951 or PBS (vehicle) were intraperitoneally injected daily from day 8 until the mice were sacrificed for analysis.

Mouse BEC-to-hepatocyte conversion model

To induce CreER recombination, the 1.5-month-old *OPN*^{CreER}*tdTomato*^{LSL} mice were intraperitoneally injected with tamoxifen (10 mg/mL) at 100 mg/kg bodyweight from day 0 to day 3. AAV8-TBG-P21 viral particles (6.75x10^{11}) were injected intravenously through tail vein at day 20. Then MCD diet (Xietong Biotech) were given from day 28 to day 43, and 10 mg/kg AV-951, 2 mg/kg rapamycin, or PBS (vehicle) were intraperitoneally injected daily from day 35 until the mice were sacrificed.

To achieve the hepatic-specific β-Catenin deletion, the 1.5-month-old *Ctnnb1*$^{flox/flox}$*tdTomato*^{LSL} mice were intravenously injected with AAV8-TBG-Cre viral particles (1.5x10^{11}) through tail vein at day 0. Then CDE diet were given from day 14 to day 28, and 10 mg/kg AV-951 or PBS (vehicle) were intraperitoneally injected daily from day 21 until the mice were sacrificed.

Antibody staining for mouse liver tissues

Mouse liver samples were fixed with 4% PFA at 4°C for 48 h, and then washed with PBS for 5 times. Then samples were dehydrated with 30% sucrose overnight and embedded with OCT at −30°C. Subsequently, the samples were subjected to frozen section. Epitope retrievals were performed by using the Quick Antigen Retrieval Solution for Frozen Sections. The liver sections were then incubated with PBTN at 4°C for 2 h. After blocking, liver sections were incubated with primary antibodies. Then the subsequent procedure is same with the zebrafish antibody staining.

QUANTIFICATION AND STATISTICAL ANALYSIS

Fluorescent intensity and areas were measured using the software ImageJ. For mouse samples, five images of each sample were randomly selected for quantification.

All statistical calculations were performed using Graphpad Prism. Unpaired two-tailed Student's t test was used for statistical analysis; $p < 0.05$ was considered statistically significant. Quantitative data were shown as means ± SEM. All figures, labels, arrows, scale bars, and outlines were assembled and drawn using the Adobe Photoshop software.